Received: 17 August 2021 | Revised: 17 August 2022 | Accepted: 27 September 2022

DOI: 10.1002/ett.4663

RESEARCH ARTICLE

WILEY

A multiple-input, multiple-output broadcasting system with space, time, polarization, and labeling diversity

Sulaiman Saleem Patel[1] | **Tahmid Quazi**[2]

[1]Department of Information Systems, Durban University of Technology, Durban, South Africa

[2]School of Engineering, University of KwaZulu-Natal, Durban, South Africa

Correspondence
Sulaiman Saleem Patel, Department of Information Systems, Durban University of Technology, Durban, South Africa.
Email: sulaimanp@dut.ac.za

Funding information
Durban University of Technology; University of KwaZulu-Natal

Abstract

Enhancing the reliability of wireless links plays an important role in addressing the digital divide between under-developed and developed nations. Diversity techniques are used in wireless communication to improve link reliability. This article presents a broadcasting system that incorporates space, time, polarization and labeling diversity. The key challenge in incorporating labeling diversity into a system is the design of appropriate bit-to-symbol mappers. The latest technique to designing bit-to-symbol mappers is to use a genetic algorithm approach, which is applicable to any generic modulation scheme. This article presents a modified genetic algorithm mapper design algorithm based on recent advances in labeling diversity evaluation theory. The proposed system is studied under ideal (uncorrelated) conditions, as well as in the presence of inter-beam and inter-antenna inference (correlated conditions). Analytical expressions are presented to model both the correlated and uncorrelated systems, and are verified via Monte Carlo simulations. When compared to the best comparable scheme at a bit-error-rate of 10^{-6}, results show that the proposed system improves performance by ≈7 dB for a 2×2 16APSK system configuration, and by ≈5 dB for both 2×4 32APSK and 2×2 64APSK system configurations. Results also show that the proposed system is highly sensitive to correlation at the transmitting node. In particular, transmit-side correlation degrades link reliability by 4 orders of magnitude for the 2×3 8APSK configuration studied at 25 dB.

Abbreviations: ABEP, average bit error probability; APSK, amplitude phase shift keying; AWGN, additive white Gaussian noise; BER, bit error rate; corr, correlation; DVB-S2X, digital video broadcasting—standard 2 extension; GA, genetic algorithm; GRV, Gaussian random variable; HSX, hypersphere swap crossover; IAI, inter-antenna interference; IBI, inter-beam interference; MGF, moment generating function; MIMO, multiple-input, multiple-output; MLD, maximum-likelihood detection; ODP, orthogonally dual-polarized; OSTBC, orthogonal space-time block code; OSTPBC, orthogonal space-time-polarization block code; PAPR, peak-to-average power ratio; PDF, probability density function; PEP, pairwise error probability; QAP, quadratic assignment problem; Rx, receive; Sim, simulation; SNR, signal-to-noise ratio; STPLD, space-time-polarization-labeling diversity; Tx, transmit; USTLD, uncoded space-time labeling diversity.

1 | INTRODUCTION

1.1 | Motivation for research

The design of current and future generations of wireless communication systems utilize multiple input (transmit) antennas andmultiple output (receive) antennas to optimize their channel capacity.[1,2] These multiple-input, multiple-output (MIMO) systems apply diversity techniques to improve their link reliability. Diversity techniques involve transmitting multiple copies of the same data across independent transmission streams.[1,3-5] Making more copies of the transmitted data available at the receiver allows for greater detection accuracy.[1,2,6,7]

The demand for these highly reliable communication links is prevalent globally for both developed and developing countries.[8] Developed countries have mature communication infrastructure and a large consumer-base for data service consumption, and hence have an ever-increasing need for ultra-reliable, high-speed wireless links. Developing countries do not have the same level of infrastructure and many of these nations have large populations living in remote or rural areas. Connecting the communities in these remote areas to the Internet is expected to produce significant socio-economic benefit to the countries as a whole.[8-10] This contributes toward bridging the digital divide[11] between developed and developing countries, and is aligned to the United Nations Sustainable Development Agenda for 2030.[12]

To achieve the desired long-range, high-reliability wireless communication links for rural communities in developing countries, satellite broadcasting has emerged as an attractive technology.[13-15] An example of the successful deployment of a satellite system of this nature was the Space4edu project, an initiative that brought Internet-based education to rural schools in South Africa.[16] Satellite broadcasting technologies have also been used to facilitate e-health services for African communities.[17,18]

Among the latest developments in enhancing satellite broadcasting systems was designing these systems using an MIMO configuration.[19-21] As documented by Arapoglou et al,[20,21] adopting an MIMO structure of satellite broadcasting is a nontrivial task due to the limited physical space available on smaller satellites. Schwartz et al[22] have addressed this limitation by proposing to use two single-antenna satellites in conjunction to act as a single dual-antenna nod0e in the system. Another technique that has been considered is the use of dual-polarized antennas.[23,24] If the polarization streams are perfectly orthogonal, a system using 1 dual-polarized transmit antenna and 1 dual-polarized receive antenna is equivalent to a 2×2 single-polarized antenna system.[23] Preliminary studies on the feasibility of MIMO satellite broadcasting have been positive. As recently as 2016, Hofmann et al[25] and Byman et al[26] documented results of implementing real-world MIMO satellite broadcast systems using each of the aforementioned configurations.

Much of the existing research on MIMO satellite broadcasting systems has adapted established terrestrial MIMO systems. One of the first terrestrial schemes to be adapted was the well-known Alamouti orthogonal space-time block code (OSTBC),[27] which was studied by Arapoglou et al[20] and Arti and Jindal[28] in the satellite context. The Alamouti OSTBC achieves spatial (space) and temporal (time) diversity.[27] More recently, other terrestrial systems that have directly improved upon the Alamouti OSTBC were also adapted for MIMO satellite broadcasting. Among these was the orthogonal space-time-polarization block code (OSTPBC) proposed by Wysocki and Wysocki,[29] which enhanced the Alamouti OSTBC by incorporating polarization diversity. The OSTPBC was extended to the context of satellite broadcast systems by Vineetha and Kirthiga[30] and Aparna et al.[31] Another notable enhancement to the terrestrial Alamouti scheme is the uncoded space-time labeling diversity (USTLD) system proposed by Xu et al.[32] This was recently extended to satellite broadcast systems by Quazi and Patel.[33]

The preceding discussion mentions that previous works improved upon the Alamouti OSTBC by incorporating either polarization diversity or labeling diversity, and have been studied for both terrestrial and satellite contexts.[29-33] In this article, a system is proposed that is derived from the Alamouti OSTBC, and incorporates both polarization *and* labeling diversity. This is dubbed the space-time-polarization-labeling-diversity (STPLD) system. The article considers the STPLD system applied in a terrestrial context, however it is envisaged that future works will be able to adapt this system to the satellite context based on its similarities with existing literature (the Alamouti OSTBC, the OSTPBC, and USTLD systems).

1.2 | Research objectives

The objectives of this research article are as follows:

- To propose a novel system design that combines four diversity techniques (spatial, temporal, polarization and labeling) to improve link reliability.
- To utilize the latest methodology for evaluating bit-to-symbol mappers that achieve labeling diversity,[33] in order to refine the latest genetic algorithm (GA) approach to bit-to-symbol mapper design.[34] The refined GA should be applied to develop bit-to-symbol mappers for the proposed STPLD system.
- To develop the process to derive closed-form numerical expressions for the STPLD system for both uncorrelated and correlated conditions in a given channel model.
- To demonstrate the derivation process using the Nakagami-q channel model and verify the closed-form expressions using Monte Carlo simulations.
- To study the link reliability and diversity order of the STPLD system and benchmark it with similar MIMO systems (ie, the Alamouti OSTBC,[27] OSTPBC,[29] and USTLD[32] schemes).
- To model the effects of inter-beam and inter-antenna interference on the STPLD system and numerically study the effect of correlation at the transmit-side and receive-side.

1.3 | Notation

This article denotes scalar quantities in italics, vectors in lowercase boldface and matrices in uppercase boldface. $|\cdot|$ and $(\cdot)!$, respectively, represent the absolute value and factorial operators. The matrix operators $\mathrm{Tr}\{\cdot\}$, $(\cdot)^T$, and $\|\cdot\|$ represent the trace, transpose and Frobenius norm, respectively. A complex number z is represented in terms of its real and imaginary parts as $z = \Re(z) + \mathrm{j}\Im(z)$, where $\mathrm{j} = \sqrt{-1}$. The complex conjugate of z is denoted with an overbar as $\bar{z}$. The binomial coefficient is represented as $\binom{n}{k} = \frac{n!}{k(n-k)!}$. Finally, the statistical expectation is denoted by the operator $\mathrm{E}\{\cdot\}$.

2 | SYSTEM MODEL

In this section, an overview of space, time, polarization, and labeling diversity is first provided. This overview focuses on how each diversity mechanism is achieved in the proposed STPLD system. Thereafter, the transmission and detection models of the STPLD system is discussed. Finally, the correlation model that will be adopted to consider the effects of inter-beam and inter-antenna interference on the system error performance is presented.

2.1 | Space, time, polarization, and labeling diversity

The proposed space-time-polarization-labeling diversity (STPLD) system considers an MIMO configuration with $N_{\mathrm{Tx}} = 2$ antennas at the STPLD transmitter and N_{Rx} antennas at the STPLD receiver. N_{Tx} is constrained to only two antennas to remain consistent with the $2 \times N_{\mathrm{Rx}}$ configuration proposed by Alamouti.[27] The use of multiple transmit and receive antennas allows the system to achieve spatial diversity.

All transmit and receive antennas are assumed to be orthogonally dual-polarized (ODP), and the polarizations used are denoted P1 and P2. There are two common configurations to ensure that antennas are ODP.[20] The first is to utilize linear polarizations (ie, a horizontal/vertical polarization pair) and the second is to utilize circular polarizations (ie, a left/right hand circular polarization pair). Arapoglou et al[20] indicate that the latter of these configurations is more robust to the effects of Faraday rotation. It is thus recommended that STPLD systems are implemented with a left/right circular polarization pair.

The use of ODP transmit antennas allows the STPLD transmitter to send a total of $2N_{\mathrm{Tx}}$ signals in any given time slot (one signal across each polarization from each antenna). Similarly, a total of $2N_{\mathrm{Rx}}$ signals are received in any given time slot by the STPLD Receiver. Thus, the $N_{\mathrm{Tx}} \times N_{\mathrm{Rx}}$ ODP antenna configuration adopted by the proposed STPLD can be modeled as a $2N_{\mathrm{Tx}} \times 2N_{\mathrm{Rx}}$ singular-polarized antenna system, effectively quadrupling the number of signal paths. The effect of more signal paths in the system is that more diversity is achieved. This comes at the expense of increased inter-beam interference (IBI),[20] which degrades the error performance of the system.

TABLE 1 Nomenclature for describing systems with labeling diversity

Term	Description
Symbol	A symbol represents the magnitude and phase used when modulating the transmission carrier in order to transmit information codewords. This is represented by a complex number.
Constellation	A constellation refers to the set of all possible symbols that may be used to encode information codewords. Constellations are commonly represented with a scatter plot of points on the complex plane, where each point represents a unique symbol.
Label	The label assigned to a symbol is the information codeword associated with that symbol. Although information codewords are binary, it is common to represent labels in decimal form for brevity.
Mapping	Mapping is the process of assigning labels to symbols using a predefined function.
Mapper	A mapper, $\omega(\cdot)$, is the mapping function which assigns labels to symbols within a constellation. The argument of ω is the label to be assigned, and its output is the corresponding symbol.

Labeling diversity, also referred to in some literature as "mapping diversity," was first proposed for bit-interleaved coded systems with iterative decoding.[35,36] The use of interleaving and coding in these systems results in higher latencies and increased power consumption. This prompted more recent studies of labeling diversity in uncoded systems.[5,32,33,37-40] Notably, Xu et al[32] proposed a scheme that applied labeling diversity to directly enhance the Alamouti OSTBC, which was named uncoded space-time labeling diversity (USTLD). It is emphasized that there are subtleties in nomenclature used when describing systems with labeling diversity, which are provided in Table 1.

In labeling diversity systems, different mappers are used to encode the same information prior to transmission. The mappers are designed such that the symbol corresponding to a given label has different neighbors when mapped by each mapper. Thus, for a labeling diversity system utilizing x mappers, each label is represented as point in a $2x$-dimensional hyperspace. The objective of mapper design is to maximize the distance between points corresponding to each label in this hyperspace. The constellation represented by each mapper is then simply a plane within the $2x$-dimensional hyperspace, and a strict constraint of the labeling diversity technique is that the symbols on each constellation remain the same, regardless of the label assigned to them.

Similar to USTLD systems,[32,33,37,38] the proposed STPLD system uses two mappers, ω_1 and ω_2. These are referred to as the "primary mapper" and "secondary mapper," respectively. For brevity, this work will refer to the constellation with labels assigned by the primary mapper as the "primary constellation." Similarly, the "secondary constellation" refers to the constellation with labels assigned by the secondary mapper. It is important to note that, in terms of the definitions in Table 1, the symbols in these constellations are identical.

Time diversity is achieved in the STPLD system by transmitting the same information codewords across 2 time slots. This makes the STPLD system more robust to burst errors.[2]

2.2 | Modulation scheme

The choice of modulation scheme for the STPLD system defines the constellation of symbols used to encode information. The STPLD system is compatible with any modulation scheme, provided that it is possible to design bit-to-symbol mappers that achieve labeling diversity. For this study, the APSK constellation is considered. APSK is a modulation scheme typically of interest in power-sensitive applications, and has been studied for tactical land mobile systems[41] and satellite communications.[33] The popularity of APSK for satellite transmissions has led to its recommendation in the latest Digital Video Broadcasting standard for satellite transmissions, DVB-S2X.[42]

APSK is considered attractive for power-sensitive applications due to it being a circular constellation. Circular constellations typically have a lower peak-to-average power ratio (PAPR) than their rectangular counterparts.[41,43] A high PAPR is undesirable, as high-gain power amplifiers at the transmitter exhibit nonlinear characteristics when operating near their saturation region.[44]

There are a wide range of APSK constellations, which may have varying levels of asymmetry.[34] For the purpose of this study, the STPLD system model considers a selection of the circular constellations recommended in the DVB-S2X standard.[42] The subset of constellations are given in Table 2 when presenting results. For all constellations in Table 2, the "+"-separated notation indicates the number of points located on each ring in the constellation structure. For example,

TABLE 2 Description of APSK constellations considered in this article

Modulation order	Structure	Definition in DVB-S2X standard[42]
8	4 + 2 + 4	Table 10a, p 25
16	8 + 8	Figure 7, p 28
32	4 + 8 + 4 + 16	Table 12d, p 30
64	4 + 12 + 20 + 28	Table 13e, p 33

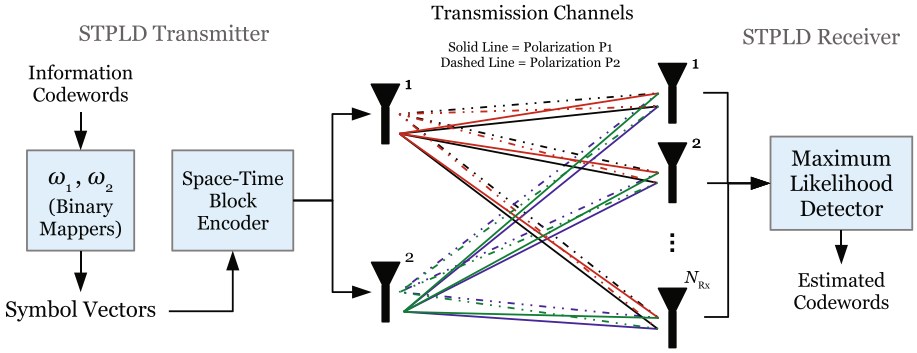

FIGURE 1 Illustration of the proposed space-time-polarization-labeling diversity system

a 4 + 12 + 16 structure would have 3 rings and a total of 32 constellation points. Four points are located on the innermost ring, 12 points are located on the middle ring and 16 points are located on the outermost ring. Table 2 also directs the reader to the constellation and codeword mapping definitions in the DVB-S2X standard. These suggested codeword mappings are used to define the primary mapper, ω_1, for the STPLD system. It should be noted that the constellations considered in this article are a wider variety of APSK configurations than was considered in previous work,[33] and that no attempts at designing bit-to-symbol mappers that achieve labeling diversity are found in literature for these constellations.

2.3 | Transmission and detection models of proposed system

An illustration of the proposed STPLD system is given in Figure 1. It is assumed that the STPLD transmitter and receiver nodes are near enough such that path-loss effects are negligible. At the transmitter, two m-bit information codewords, ℓ_1 and ℓ_2, are mapped to complex symbols from a M-ary constellation and transmitted across two time slots, where $M = 2^m$. To achieve labeling diversity, a different mapping function to select symbols is employed in each time slot, that is, mapper ω_k is employed in time slot k, where $k \in [1:2]$. The constellations considered in this article are a selection of APSK constellations from the latest DVB-S2X standard,[42] as discussed in Section 2.2. The design of the labeling diversity mappers for these constellations is detailed in Section 4. The system is designed such that a copy of each symbol $\omega_k(\ell_j)$, $j \in [1:2]$, is transmitted from each antenna and over each polarization during time slot $k, k \in [1:2]$.

At the receiver, the $2N_{\text{Rx}} \times 1$ received signal vector, $\mathbf{y}$, during time slot k, where $k \in [1:2]$, is given by:

$$\begin{aligned}\mathbf{y}_k &= \begin{bmatrix} y_{\text{P1}_k}^{(1)} & y_{\text{P2}_k}^{(1)} & y_{\text{P1}_k}^{(2)} & y_{\text{P2}_k}^{(2)} & \cdots & y_{\text{P1}_k}^{(N_{\text{Rx}})} & y_{\text{P2}_k}^{(N_{\text{Rx}})} \end{bmatrix}^{\text{T}} \\ &= \sqrt{\frac{E_{\text{Tx}}}{4E_\omega E_{\text{n}}}} \begin{bmatrix} \mathbf{h}_{\text{P1}_k}^{(1)} & \mathbf{h}_{\text{P2}_k}^{(1)} & \mathbf{h}_{\text{P1}_k}^{(2)} & \mathbf{h}_{\text{P2}_k}^{(2)} \end{bmatrix} \begin{bmatrix} \omega_k(\ell_1) \\ \omega_k(\ell_2) \\ \omega_k(\ell_2) \\ \omega_k(\ell_1) \end{bmatrix} + \mathbf{n}_k, \end{aligned} \tag{1}$$

where $y_{\mathrm{P1}}^{(a)}$ represents the signal received by the ath receive antenna with polarization P1, where $a \in [1 : N_{\mathrm{Rx}}]$, and similarly for $y_{\mathrm{P2}}^{(a)}$. E_{Tx} is the total energy of the transmitted signal, which is split equally across each polarization and each transmit antenna. $E_\omega = \frac{1}{M}\sum_{i=0}^{M-1}|\omega_1(i)|^2 = \frac{1}{M}\sum_{i=0}^{M-1}|\omega_2(i)|^2$ is a factor to ensure that transmitted symbols are power-normalized and E_n is the expected energy of additive white Gaussian noise (AWGN) at the receiver. These factors may be written more compactly by defining the total average signal-to-noise ratio (SNR) of the system, $\gamma = \frac{E_{\mathrm{Tx}}}{E_\omega E_{\mathrm{n}}}$. This allows the entries of noise vector, $\mathbf{n}$, to be modeled as following a complex normal distribution with zero mean and unit variance. The $2N_{\mathrm{Rx}} \times 1$ vectors $\mathbf{h}_{\mathrm{P1}}^{(b)}$ and $\mathbf{h}_{\mathrm{P2}}^{(b)}$ represent the narrowband multipath fading experienced by the symbols transmitted from transmit antenna b, $b \in [1 : 2]$, with the respective polarizations P1 and P2. It is assumed that the fading is fast, frequency-flat and that it follows a Nakagami-q amplitude distribution with zero mean and unit variance. The Nakagami-q fading model is a generalization of the Rayleigh fading model,[45] and gives insight into the worst-case error performance of the STPLD system.[38] The fading parameter, q, lies in the continuous range $0 \le q \le 1$ and is the energy ratio of the quadrature component of the fading to its in-phase component.[45] The boundary conditions of q correspond to the cases of single-sided Gaussian fading ($q = 0$) and Rayleigh fading ($q = 1$), as discussed by Simon and Alouini.[7] The phase distribution of both the noise and fading vectors entries in (1) is assumed uniform.

To estimate the transmitted codewords, the base station employs maximum likelihood detection (MLD). Under the assumption that accurate channel state information is available at the receiver, the detected codewords, $\tilde{\ell}_1$ and $\tilde{\ell}_2$, are given by:

$$\tilde{\ell}_1, \tilde{\ell}_2 = \underset{l_1, l_2 \in [0:M-1]}{\operatorname{argmin}} \left\| \mathbf{y}_1 - \sqrt{\frac{E_{\mathrm{Tx}}}{4E_\omega E_{\mathrm{n}}}} \begin{bmatrix} \mathbf{h}_{\mathrm{P1}_1}^{(1)} & \mathbf{h}_{\mathrm{P2}_1}^{(1)} & \mathbf{h}_{\mathrm{P1}_1}^{(2)} & \mathbf{h}_{\mathrm{P2}_1}^{(2)} \end{bmatrix} \begin{bmatrix} \omega_1(l_1) \\ \omega_1(l_2) \\ \omega_1(l_2) \\ \omega_1(l_1) \end{bmatrix} \right\|^2 + \left\| \mathbf{y}_2 - \sqrt{\frac{E_{\mathrm{Tx}}}{4E_\omega E_{\mathrm{n}}}} \begin{bmatrix} \mathbf{h}_{\mathrm{P1}_2}^{(1)} & \mathbf{h}_{\mathrm{P2}_2}^{(1)} & \mathbf{h}_{\mathrm{P1}_2}^{(2)} & \mathbf{h}_{\mathrm{P2}_2}^{(2)} \end{bmatrix} \begin{bmatrix} \omega_2(l_1) \\ \omega_2(l_2) \\ \omega_2(l_2) \\ \omega_2(l_1) \end{bmatrix} \right\|^2, \tag{2}$$

where l_1 and l_2 are candidate codewords to be evaluated during the detection. It is apparent that the complexity of this MLD described by (2) is $\mathcal{O}\left(M^2\right)$, where $\mathcal{O}(\cdot)$ is the "order of" operator commonly used in the upper-bound analysis of algorithmic complexity.[46]

2.4 | Correlation model

This article adopts the separable Kronecker correlation model[47] to model the effect of inter-antenna and inter-beam interference on the STPLD system. The Kronecker model relates the correlated channel matrix in the kth time slot, $\begin{bmatrix} \mathbf{h}_{\mathrm{P1}_k}^{(1)} & \mathbf{h}_{\mathrm{P2}_k}^{(1)} & \mathbf{h}_{\mathrm{P1}_k}^{(2)} & \mathbf{h}_{\mathrm{P2}_k}^{(2)} \end{bmatrix}$, to a virtual, uncorrelated channel matrix, $\begin{bmatrix} \grave{\mathbf{h}}_{\mathrm{P1}_k}^{(1)} & \grave{\mathbf{h}}_{\mathrm{P2}_k}^{(1)} & \grave{\mathbf{h}}_{\mathrm{P1}_k}^{(2)} & \grave{\mathbf{h}}_{\mathrm{P2}_k}^{(2)} \end{bmatrix}$, a transmitter-side correlation matrix ($\mathbf{C}_{\mathrm{Tx}}$) and a receiver-side correlation matrix ($\mathbf{C}_{\mathrm{Rx}}$) according to:

$$\begin{bmatrix} \mathbf{h}_{\mathrm{P1}_k}^{(1)} & \mathbf{h}_{\mathrm{P2}_k}^{(1)} & \mathbf{h}_{\mathrm{P1}_k}^{(2)} & \mathbf{h}_{\mathrm{P2}_k}^{(2)} \end{bmatrix} = \mathbf{C}_{\mathrm{Rx}}^{\frac{1}{2}} \begin{bmatrix} \grave{\mathbf{h}}_{\mathrm{P1}_k}^{(1)} & \grave{\mathbf{h}}_{\mathrm{P2}_k}^{(1)} & \grave{\mathbf{h}}_{\mathrm{P1}_k}^{(2)} & \grave{\mathbf{h}}_{\mathrm{P2}_k}^{(2)} \end{bmatrix} \left(\mathbf{C}_{\mathrm{Tx}}^{\frac{1}{2}} \right)^{\mathrm{T}}, \quad k \in [1 : 2]. \tag{3}$$

As this article considers the Nakagami-q fading model, the amplitude of each entry of the virtual, uncorrelated channel matrix in (3) follows a Nakagami-q distribution with zero mean and unit variance.

Each correlation matrix is defined in terms of the signal paths from each antenna, utilizing each polarization. As an example, the $2N_{\mathrm{Tx}} \times 2N_{\mathrm{Tx}}$ transmit-side correlation matrix is defined as:

$$\mathbf{C}_{\mathrm{Tx}} = \begin{bmatrix} 1 & \rho_{\mathrm{Tx}}^{(P1_1,P2_1)} & \rho_{\mathrm{Tx}}^{(P1_1,P1_2)} & \rho_{\mathrm{Tx}}^{(P1_1,P2_2)} \\ \rho_{\mathrm{Tx}}^{(P2_1,P1_1)} & 1 & \rho_{\mathrm{Tx}}^{(P2_1,P1_2)} & \rho_{\mathrm{Tx}}^{(P2_1,P2_2)} \\ \rho_{\mathrm{Tx}}^{(P1_2,P1_1)} & \rho_{\mathrm{Tx}}^{(P1_2,P2_1)} & 1 & \rho_{\mathrm{Tx}}^{(P1_2,P2_2)} \\ \rho_{\mathrm{Tx}}^{(P2_2,P1_1)} & \rho_{\mathrm{Tx}}^{(P2_2,P2_1)} & \rho_{\mathrm{Tx}}^{(P2_2,P1_2)} & 1 \end{bmatrix},$$

where $\rho_{\mathrm{Tx}}^{(X_i,Y_j)}$, $X, Y \in \{P1, P2\}, i, j \in [1 : 2]$, represents the correlation coefficient between the signal sent across polarization X from transmit antenna i and signal sent across polarization Y from transmit antenna j. The correlation coefficients are complex-symmetrical such that $\rho_{\mathrm{Tx}}^{(X_i,Y_j)} = \overline{\rho}_{\mathrm{Tx}}^{(Y_j,X_i)}$. The entries of the correlation matrix model both IBI and inter-antenna interference (IAI) that may be present in the STPLD system. In (4), the correlation coefficient $\rho_{\mathrm{Tx}}^{(P1_1,P2_1)}$ is representative of the IBI between the P1-polarized and P2-polarized signals broadcast from transmit antenna 1. Similarly, $\rho_{\mathrm{Tx}}^{(P1_1,P1_2)}$ represents the IAI between the P1-polarized signals from transmit antennas 1 and 2. $\rho_{\mathrm{Tx}}^{(P1_1,P2_2)}$ is an example of an entry that models both IAI and IBI, as it represents the correlation between the P1-polarized signal transmitted from antenna 1 and the P2-polarized signal transmitted from antenna 2. Similar to (4), the $2N_{\mathrm{Rx}} \times 2N_{\mathrm{Rx}}$ receive-side correlation matrix, $\mathbf{C}_{\mathrm{Rx}}$, is defined in terms of correlation coefficients $\rho_{\mathrm{Rx}}^{(X_i,Y_j)}$, $X, Y \in \{P1, P2\}$, $i, j \in [1 : N_{\mathrm{Rx}}]$.

When constructing the antenna correlation matrix, three general cases may be considered: (i) the case where there is only IBI, (ii) the case where there is only IAI, and (iii) the case where there is both IBI and IAI. The following discussion show how the receive-side antenna correlation matrix is constructed for each of the above cases, assuming three dual-polarized receive antennas. The reasoning applied may be similarly extended for the transmit-side correlation matrix in systems with more than two transmit antennas.

2.4.1 | Case 1: Only inter-beam interference

Under the assumption that all antennas are manufactured identically, the IBI correlation coefficients for each antenna are the same. Denoting these as ρ^{IBI}, and assuming no IAI, the receive-side correlation matrix is given by:

$$\mathbf{C}_{\mathrm{Rx,\ only\ IBI}} = \begin{bmatrix} 1 & \rho_{\mathrm{Rx}}^{\mathrm{IBI}} & 0 & 0 & 0 & 0 \\ \rho_{\mathrm{Rx}}^{\mathrm{IBI}} & 1 & 0 & 0 & 0 & 0 \\ 0 & 0 & 1 & \rho_{\mathrm{Rx}}^{\mathrm{IBI}} & 0 & 0 \\ 0 & 0 & \rho_{\mathrm{Rx}}^{\mathrm{IBI}} & 1 & 0 & 0 \\ 0 & 0 & 0 & 0 & 1 & \rho_{\mathrm{Rx}}^{\mathrm{IBI}} \\ 0 & 0 & 0 & 0 & \rho_{\mathrm{Rx}}^{\mathrm{IBI}} & 1 \end{bmatrix}. \tag{5}$$

$\mathbf{C}_{\mathrm{Rx,\ only\ IBI}}$ is of a similar structure to the dual-correlation matrix presented by Reşat and Özyurt.[48] This is reasonable, as the signals received by each of the ODP antennas will be dual-correlated.

2.4.2 | Case 2: Only inter-antenna interference

Under the assumption that only IAI is present in the system, correlation exists between the P1-polarized and P2-polarized beams from each antenna. Since IAI is independent of polarization, the IAI experienced by the P1-polarized and P2-polarized beams are the same, and denoted as ρ^{IAI}. This may alternately be viewed as modeling only co-polar IAI. A common method to express the correlation matrix for systems with IAI is to use the exponential correlation model (ECM).[48-52] Reşat and Özyurt[48] discuss that the ECM is more reasonable for modeling antenna correlation in real-world systems than the alternative constant and dual-correlation models. Using the ECM and assuming no IBI, the receive-side correlation matrix becomes:

$$\mathbf{C}_{\text{Rx, only IAI}} = \begin{bmatrix} 1 & 0 & \rho_{\text{Rx}}^{\text{IAI}} & 0 & \left(\rho_{\text{Rx}}^{\text{IAI}}\right)^2 & 0 \\ 0 & 1 & 0 & \rho_{\text{Rx}}^{\text{IAI}} & 0 & \left(\rho_{\text{Rx}}^{\text{IAI}}\right)^2 \\ \rho_{\text{Rx}}^{\text{IAI}} & 0 & 1 & 0 & \rho_{\text{Rx}}^{\text{IAI}} & 0 \\ 0 & \rho_{\text{Rx}}^{\text{IAI}} & 0 & 1 & 0 & \rho_{\text{Rx}}^{\text{IAI}} \\ \left(\rho_{\text{Rx}}^{\text{IAI}}\right)^2 & 0 & \rho_{\text{Rx}}^{\text{IAI}} & 0 & 1 & 0 \\ 0 & \left(\rho_{\text{Rx}}^{\text{IAI}}\right)^2 & 0 & \rho_{\text{Rx}}^{\text{IAI}} & 0 & 1 \end{bmatrix}. \tag{6}$$

2.4.3 | Case 3: Both inter-antenna and inter-beam interference

When modeling both IAI and IBI, the statistical definition of the correlation coefficient provided by Akoun and Xu[53(eq2)] is used. Observing that IAI and IBI are independent, it can be shown that the correlation coefficient for a channel element that experiences both IAI and IBI (ie, the cross-polar IAI correlation coefficient) is the product of the correlation coefficients arising from only IAI and only IBI. Thus, using (5) and (6), the receive-side correlation matrix becomes:

$$\begin{aligned} \mathbf{C}_{\text{Rx, IAI, and IBI}} &= \mathbf{C}_{\text{Rx, only IAI}} + \mathbf{C}_{\text{Rx, only IBI}} + \begin{bmatrix} -1 & 0 & 0 & \rho_{\text{Rx}}^{\text{IBI}}\rho_{\text{Rx}}^{\text{IAI}} & 0 & \rho_{\text{Rx}}^{\text{IBI}}\left(\rho_{\text{Rx}}^{\text{IAI}}\right)^2 \\ 0 & -1 & \rho_{\text{Rx}}^{\text{IBI}}\rho_{\text{Rx}}^{\text{IAI}} & 0 & \rho_{\text{Rx}}^{\text{IBI}}\left(\rho_{\text{Rx}}^{\text{IAI}}\right)^2 & 0 \\ 0 & \rho_{\text{Rx}}^{\text{IBI}}\rho_{\text{Rx}}^{\text{IAI}} & -1 & 0 & 0 & \rho_{\text{Rx}}^{\text{IBI}}\rho_{\text{Rx}}^{\text{IAI}} \\ \rho_{\text{Rx}}^{\text{IBI}}\rho_{\text{Rx}}^{\text{IAI}} & 0 & 0 & -1 & \rho_{\text{Rx}}^{\text{IBI}}\rho_{\text{Rx}}^{\text{IAI}} & 0 \\ 0 & \rho_{\text{Rx}}^{\text{IBI}}\left(\rho_{\text{Rx}}^{\text{IAI}}\right)^2 & 0 & \rho_{\text{Rx}}^{\text{IBI}}\rho_{\text{Rx}}^{\text{IAI}} & -1 & 0 \\ \rho_{\text{Rx}}^{\text{IBI}}\left(\rho_{\text{Rx}}^{\text{IAI}}\right)^2 & 0 & \rho_{\text{Rx}}^{\text{IBI}}\rho_{\text{Rx}}^{\text{IAI}} & 0 & 0 & -1 \end{bmatrix} \\ &= \begin{bmatrix} 1 & \rho_{\text{Rx}}^{\text{IBI}} & \rho_{\text{Rx}}^{\text{IAI}} & \rho_{\text{Rx}}^{\text{IBI}}\rho_{\text{Rx}}^{\text{IAI}} & \left(\rho_{\text{Rx}}^{\text{IAI}}\right)^2 & \rho_{\text{Rx}}^{\text{IBI}}\left(\rho_{\text{Rx}}^{\text{IAI}}\right)^2 \\ \rho_{\text{Rx}}^{\text{IBI}} & 1 & \rho_{\text{Rx}}^{\text{IBI}}\rho_{\text{Rx}}^{\text{IAI}} & \rho_{\text{Rx}}^{\text{IAI}} & \rho_{\text{Rx}}^{\text{IBI}}\left(\rho_{\text{Rx}}^{\text{IAI}}\right)^2 & \left(\rho_{\text{Rx}}^{\text{IAI}}\right)^2 \\ \rho_{\text{Rx}}^{\text{IAI}} & \rho_{\text{Rx}}^{\text{IBI}}\rho_{\text{Rx}}^{\text{IAI}} & 1 & \rho_{\text{Rx}}^{\text{IBI}} & \rho_{\text{Rx}}^{\text{IAI}} & \rho_{\text{Rx}}^{\text{IBI}}\rho_{\text{Rx}}^{\text{IAI}} \\ \rho_{\text{Rx}}^{\text{IBI}}\rho_{\text{Rx}}^{\text{IAI}} & \rho_{\text{Rx}}^{\text{IAI}} & \rho_{\text{Rx}}^{\text{IBI}} & 1 & \rho_{\text{Rx}}^{\text{IBI}}\rho_{\text{Rx}}^{\text{IAI}} & \rho_{\text{Rx}}^{\text{IAI}} \\ \left(\rho_{\text{Rx}}^{\text{IAI}}\right)^2 & \rho_{\text{Rx}}^{\text{IBI}}\left(\rho_{\text{Rx}}^{\text{IAI}}\right)^2 & \rho_{\text{Rx}}^{\text{IAI}} & \rho_{\text{Rx}}^{\text{IBI}}\rho_{\text{Rx}}^{\text{IAI}} & 1 & \rho_{\text{Rx}}^{\text{IBI}} \\ \rho_{\text{Rx}}^{\text{IBI}}\left(\rho_{\text{Rx}}^{\text{IAI}}\right)^2 & \left(\rho_{\text{Rx}}^{\text{IAI}}\right)^2 & \rho_{\text{Rx}}^{\text{IBI}}\rho_{\text{Rx}}^{\text{IAI}} & \rho_{\text{Rx}}^{\text{IAI}} & \rho_{\text{Rx}}^{\text{IBI}} & 1 \end{bmatrix}. \end{aligned} \tag{7}$$

The authors note that the additional matrix introduced takes into account cross-polar IAI. Negatives were introduced along the primary diagonal of this term to ensure that the final expression has a unitary primary diagonal.

3 | ANALYSIS OF ERROR PERFORMANCE

3.1 | Uncorrelated error performance

Due to the STPLD system achieving multiple forms of diversity, it is expected that the wireless link will be very reliable at high SNRs. It is thus reasonable to assume that in the high-SNR region, the ABEP of the STPLD system may be approximated by the probability of only a single codeword being detected erroneously. This is in agreement with the assumption used in other literature when analyzing space-time block coded systems with labeling diversity.[5,32,37,38] Under this assumption, the following derivation considers the case (without loss of generality) wherein codeword ℓ_2 is detected correctly and codeword ℓ_1 is detected erroneously as l_1. The union bound of the ABEP for the uncorrelated STPLD system is thus given by:

$$\mathcal{P}_e \leq \frac{1}{M}\sum_{\ell_1=0}^{M-1}\sum_{l_1=0}^{M-1}\frac{\Delta(\ell_1, l_1)}{m}\mathcal{P}(\ell_1 \to l_1), \tag{8}$$

where $\mathcal{P}(\ell_1 \to l_1)$ is the pairwise error probability (PEP) that transmitted codeword ℓ_1 is incorrectly detected as codeword l_1, and $\Delta(\ell_1, l_1)$ is the number of bit errors between ℓ_1 and l_1.

Given the assumption that only ℓ_1 is detected incorrectly at the receiver, the PEP conditioned on perfect knowledge of all channels, across both polarizations and both time slots, is given by:

$$
\begin{aligned}
&\mathcal{P}\left(\ell_1 \to l_1 \mid \mathbf{h}_{\mathrm{P1}_1}^{(1)}, \mathbf{h}_{\mathrm{P2}_1}^{(1)}, \mathbf{h}_{\mathrm{P1}_1}^{(2)}, \mathbf{h}_{\mathrm{P2}_1}^{(2)}, \mathbf{h}_{\mathrm{P1}_2}^{(1)}, \mathbf{h}_{\mathrm{P2}_2}^{(1)}, \mathbf{h}_{\mathrm{P1}_2}^{(2)}, \mathbf{h}_{\mathrm{P2}_2}^{(2)}\right) \\
&= \mathcal{P}\left(\sum_{k=1}^{2}\left\| \mathbf{y}_k - \sqrt{\frac{E_{\mathrm{Tx}}}{4E_\omega E_{\mathrm{n}}}}\begin{bmatrix}\mathbf{h}_{\mathrm{P1}_k}^{(1)} & \mathbf{h}_{\mathrm{P2}_k}^{(1)} & \mathbf{h}_{\mathrm{P1}_k}^{(2)} & \mathbf{h}_{\mathrm{P2}_k}^{(2)}\end{bmatrix}\begin{bmatrix}\omega_k(l_1)\\ \omega_k(l_2)\\ \omega_k(l_2)\\ \omega_k(l_1)\end{bmatrix}\right\|^2\right. \\
&\left.< \sum_{k=1}^{2}\left\| \mathbf{y}_k - \sqrt{\frac{E_{\mathrm{Tx}}}{4E_\omega E_{\mathrm{n}}}}\begin{bmatrix}\mathbf{h}_{\mathrm{P1}_k}^{(1)} & \mathbf{h}_{\mathrm{P2}_k}^{(1)} & \mathbf{h}_{\mathrm{P1}_k}^{(2)} & \mathbf{h}_{\mathrm{P2}_k}^{(2)}\end{bmatrix}\begin{bmatrix}\omega_k(\ell_1)\\ \omega_k(\ell_2)\\ \omega_k(\ell_2)\\ \omega_k(\ell_1)\end{bmatrix}\right\|^2\right) \\
&= \mathcal{P}\left(\sum_{k=1}^{2}\left\| \sqrt{\frac{E_{\mathrm{Tx}}}{4E_\omega E_{\mathrm{n}}}}\begin{bmatrix}\mathbf{h}_{\mathrm{P1}_k}^{(1)} & \mathbf{h}_{\mathrm{P2}_k}^{(1)} & \mathbf{h}_{\mathrm{P1}_k}^{(2)} & \mathbf{h}_{\mathrm{P2}_k}^{(2)}\end{bmatrix}\begin{bmatrix}\omega_k(\ell_1)-\omega_k(l_1)\\ \omega_k(\ell_2)-\omega_k(l_2)\\ \omega_k(\ell_2)-\omega_k(l_2)\\ \omega_k(\ell_1)-\omega_k(l_1)\end{bmatrix} + \mathbf{n}_k\right\|^2 < \|\mathbf{n}_1\|^2 + \|\mathbf{n}_2\|^2\right), \text{ Assumption} \Rightarrow l_2 = \ell_2
\end{aligned}
\tag{9}
$$

$$
= \mathcal{P}\left(\sum_{k=1}^{2}\left\| \sqrt{\frac{E_{\mathrm{Tx}}}{4E_\omega E_{\mathrm{n}}}}\begin{bmatrix}\mathbf{h}_{\mathrm{P1}_k}^{(1)} & \mathbf{h}_{\mathrm{P2}_k}^{(1)} & \mathbf{h}_{\mathrm{P1}_k}^{(2)} & \mathbf{h}_{\mathrm{P2}_k}^{(2)}\end{bmatrix}\begin{bmatrix}\omega_k(\ell_1)-\omega_k(l_1)\\ 0\\ 0\\ \omega_k(\ell_1)-\omega_k(l_1)\end{bmatrix} + \mathbf{n}_k\right\|^2 < \|\mathbf{n}_1\|^2 + \|\mathbf{n}_2\|^2\right) \tag{10}
$$

$$
= \mathcal{P}\left(\sum_{k=1}^{2}\left\| \sqrt{\frac{E_{\mathrm{Tx}}}{4E_\omega E_{\mathrm{n}}}}\left(\mathbf{h}_{\mathrm{P1}_k}^{(1)} + \mathbf{h}_{\mathrm{P2}_k}^{(2)}\right)\varepsilon_k^{(\ell_1,l_1)} + \mathbf{n}_k\right\|^2 < \|\mathbf{n}_1\|^2 + \|\mathbf{n}_2\|^2\right). \tag{11}
$$

It is highlighted that, due to the assumption that only ℓ_1 is detected erroneously, $\ell_2 = l_2$ where l_2 is the estimated codeword corresponding to ℓ_2 at the receiver. Therefore, $\omega_k(\ell_2) = \omega_k(l_2)$ in (9), which results in the zero vector elements in (10).

In (11), $\varepsilon_k^{(\ell_1,l_1)}$ represents the difference between the constellation points corresponding to labels ℓ_1 and l_1 when mapped using ω_k. In general, the difference between labels a and b is defined by:

$$
\varepsilon_k^{(a,b)} = \omega_k(a) - \omega_k(b); \quad k \in [1:2],\ a, b \in [0:M-1]. \tag{12}
$$

Using equation (5.1.5) from Meyer[54] and substituting $\mathbf{g}_k = \sqrt{\frac{E_{\mathrm{Tx}}}{4E_\omega E_{\mathrm{n}}}}\left(\mathbf{h}_{\mathrm{P1}_k}^{(1)} + \mathbf{h}_{\mathrm{P2}_k}^{(2)}\right)\varepsilon_k^{(\ell_1,l_1)}$ to simplify notation, the summed terms on the lesser side of the inequality in (11) may be written as:

$$
\begin{aligned}
\sum_{k=1}^{2}\left\| \sqrt{\frac{E_{\mathrm{Tx}}}{4E_\omega E_{\mathrm{n}}}}\left(\mathbf{h}_{\mathrm{P1}_k}^{(1)} + \mathbf{h}_{\mathrm{P2}_k}^{(2)}\right)\varepsilon_k^{(\ell_1,l_1)} + \mathbf{n}_k\right\|^2 &= \sum_{k=1}^{2}\left\|\mathbf{g}_k + \mathbf{n}_k\right\|^2 \\
&= \sum_{k=1}^{2}\left[\|\mathbf{g}_k\|^2 + \|\mathbf{n}_k\|^2 + 2\Re\left(\overline{\mathbf{n}}_k^{\mathrm{T}}\,\mathbf{g}_k\right)\right].
\end{aligned}
\tag{13}
$$

Since (11) is conditioned on perfect knowledge of all channels, $\overline{\mathbf{n}}_k^{\mathrm{T}}\mathbf{g}_k,\ k \in [1:2]$, represents the sum of $2N_{\mathrm{Rx}}$ complex Gaussian random variables (GRVs). Each GRV, has zero mean and variance $|g_{j,k}|^2$, where $g_{j,k}$ represents the jth element

of $\mathbf{g}_k$ and $j \in [1 : 2N_{\mathrm{Rx}}]$. Hence, it may be deduced that $\sum_{k=1}^{2} \Re\left(\overline{\mathbf{n}}_k^{\mathrm{T}}\, \mathbf{g}_k\right)$ is a complex GRV with zero mean and variance $\sigma_{\mathrm{GRV}}^2 = \frac{1}{2}\sum_{k=1}^{2}\|\mathbf{g}_k\|^2$.

The conditional PEP in (11) may thus be expressed as:

$$\begin{aligned}
\mathcal{P}\left(\ell_1 \to l_1 \mid \mathbf{h}_{\mathrm{P1}_1}^{(1)}, \mathbf{h}_{\mathrm{P2}_1}^{(1)}, \mathbf{h}_{\mathrm{P1}_1}^{(2)}, \mathbf{h}_{\mathrm{P2}_1}^{(2)}, \mathbf{h}_{\mathrm{P1}_2}^{(1)}, \mathbf{h}_{\mathrm{P2}_2}^{(1)}, \mathbf{h}_{\mathrm{P1}_2}^{(2)}, \mathbf{h}_{\mathrm{P2}_2}^{(2)}\right) &= \mathcal{P}\left(\sum_{k=1}^{2}\left[\|\mathbf{g}_k\|^2 + \|\mathbf{n}_k\|^2 + 2\Re\left(\overline{\mathbf{n}}_k^{\mathrm{T}}\, \mathbf{g}_k\right)\right] < \|\mathbf{n}_1\|^2 + \|\mathbf{n}_2\|^2\right) \\
&= \mathcal{P}\left(\sum_{k=1}^{2}\Re\left(\overline{\mathbf{n}}_k^{\mathrm{T}}\, \mathbf{g}_k\right) + \frac{\sum_{k=1}^{2}\|\mathbf{g}_k\|^2}{2} < 0\right) \\
&= \mathcal{Q}\left(\frac{\sum_{k=1}^{2}\|\mathbf{g}_k\|^2}{2\sqrt{\sigma_{\mathrm{GRV}}^2}}\right) \\
&= \mathcal{Q}\left(\sqrt{\frac{1}{2}\sum_{k=1}^{2}\|\mathbf{g}_k\|^2}\right) \qquad (14) \\
&= \mathcal{Q}\left(\sqrt{\frac{1}{2}\sum_{j=1}^{2N_{\mathrm{Rx}}}\sum_{k=1}^{2}\alpha_{j,k}^2}\right), \qquad (15)
\end{aligned}$$

where $\mathcal{Q}(x) = \frac{1}{\pi}\int_0^{\frac{\pi}{2}} \exp\left(-\frac{x^2}{2\sin^2(y)}\right) \mathrm{d}y$ is the Gaussian Q-function in the form presented by Craig.[55] In the penultimate step of the above set of equations, (15) is obtained by expanding the vector Frobenius norms in (14) and defining the amplitude $\alpha_{j,k} = |g_{j,k}|$.

Since the Q-function has finite bounds of integration, it may be solved numerically using a trapezoidal approximation.[32,38] Hence, (15) may be expressed as:

$$\begin{aligned}
\mathcal{Q}\left(\sqrt{\frac{1}{2}\sum_{j=1}^{2N_{\mathrm{Rx}}}\sum_{k=1}^{2}\alpha_{j,k}^2}\right) &= \frac{1}{\pi}\int_0^{\frac{\pi}{2}} \exp\left(-\sum_{j=1}^{2N_{\mathrm{Rx}}}\sum_{k=1}^{2}\frac{\alpha_{j,k}^2}{4\sin^2(y)}\right)\mathrm{d}y \\
&= \frac{1}{\pi}\prod_{j=1}^{2N_{\mathrm{Rx}}}\prod_{k=1}^{2}\int_0^{\frac{\pi}{2}} \exp\left(-\frac{\alpha_{j,k}^2}{4\sin^2(y)}\right)\mathrm{d}y \\
&\approx \frac{1}{4r}\prod_{j=1}^{2N_{\mathrm{Rx}}} \exp\left(-\frac{\alpha_{j,1}^2}{4}\right)\exp\left(-\frac{\alpha_{j,2}^2}{4}\right) + \frac{1}{2r}\prod_{j=1}^{2N_{\mathrm{Rx}}}\sum_{R=1}^{r-1} \exp\left(-\frac{\alpha_{j,1}^2}{4\sin^2\left(\frac{R\pi}{2r}\right)}\right)\exp\left(-\frac{\alpha_{j,2}^2}{4\sin^2\left(\frac{R\pi}{2r}\right)}\right), \qquad (16)
\end{aligned}$$

where r is a sufficiently large integer to allow the trapezoidal approximation to converge to the integral result.

The next step of this derivation is to obtain the unconditioned PEP, $\mathcal{P}(\ell_1 \to l_1)$, as required by the union bound expression in (8). This is done by integrating (16) over the probability density function (PDF) of element $\alpha_{j,k}$, denoted as $\mathcal{F}_{\alpha_{j,k}}(\cdot)$. The resulting expression for the unconditioned PEP is:

$$\begin{aligned}
\mathcal{P}(\ell_1 \to l_1) \approx \frac{1}{4r}\prod_{j=1}^{2N_{\mathrm{Rx}}}\int_0^{\infty} \exp\left(-\frac{\alpha_{j,1}^2}{4}\right)\mathcal{F}_{\alpha_{j,1}}\left(\alpha_{j,1}\right)\,\mathrm{d}\alpha_{j,1}\int_0^{\infty} \exp\left(-\frac{\alpha_{j,2}^2}{4}\right)\mathcal{F}_{\alpha_{j,2}}\left(\alpha_{j,2}\right)\,\mathrm{d}\alpha_{j,2} \\
+ \frac{1}{2r}\prod_{j=1}^{2N_{\mathrm{Rx}}}\sum_{R=1}^{r-1}\int_0^{\infty} \exp\left(-\frac{\alpha_{j,1}^2}{4\sin^2\left(\frac{R\pi}{2r}\right)}\right)\mathcal{F}_{\alpha_{j,1}}\left(\alpha_{j,1}\right)\,\mathrm{d}\alpha_{j,1}\int_0^{\infty} \exp\left(-\frac{\alpha_{j,2}^2}{4\sin^2\left(\frac{R\pi}{2r}\right)}\right)\mathcal{F}_{\alpha_{j,2}}\left(\alpha_{j,2}\right)\,\mathrm{d}\alpha_{j,2}. \qquad (17)
\end{aligned}$$

From the earlier definition of $\mathbf{g}_k$, it follows that the amplitude $\alpha_{j,k} = |g_{j,k}| = \left|\sqrt{\frac{E_{\mathrm{Tx}}}{4E_{\omega}E_{\mathrm{n}}}}\left(h_{j,\mathrm{P1}_k}^{(1)} + h_{j,\mathrm{P2}_k}^{(2)}\right)\varepsilon_k^{(\ell_1,l_1)}\right|, j \in [1 : 2N_{\mathrm{Rx}}], k \in [1 : 2]$, where $h_{j,\mathrm{P1}_k}^{(1)}$ represents the jth element of matrix $\mathbf{h}_{\mathrm{P1}_k}^{(1)}$, and similarly for $h_{j,\mathrm{P2}_k}^{(2)}$.

As per the system model described in Section 2, the amplitude of all fading coefficients in this study are assumed to follow a Nakagami-q distribution with zero mean and unit variance. In the case of uncorrelated channels, $\alpha_{j,k}$ also follows a Nakagami-q distribution with zero mean and variance $\sigma^2_{\alpha_{j,k}}$, which is given by (18). In the case of a different channel model, the amplitude of the fading coefficient would change and the ensuing derivation would need adaptation.

$$\begin{aligned}\sigma^2_{\alpha_{j,k}} &= \mathrm{E}\left\{ \left| \sqrt{\frac{E_{\mathrm{Tx}}}{4E_\omega E_{\mathrm{n}}}} \left(h^{(1)}_{j,\mathrm{P1}_k} + h^{(2)}_{j,\mathrm{P2}_k} \right) \varepsilon^{(\ell_1,l_1)}_k \right|^2 \right\} \\ &= \frac{E_{\mathrm{Tx}}}{4E_\omega E_{\mathrm{n}}} \left| \varepsilon^{(\ell_1,l_1)}_k \right|^2 \times \mathrm{E}\left\{ \left| h^{(1)}_{j,\mathrm{P1}_k} + h^{(2)}_{j,\mathrm{P2}_k} \right|^2 \right\} \\ &= \frac{E_{\mathrm{Tx}}}{4E_\omega E_{\mathrm{n}}} \left| \varepsilon^{(\ell_1,l_1)}_k \right|^2 \times 2 \\ &= \frac{E_{\mathrm{Tx}}}{2E_\omega E_{\mathrm{n}}} \left| \varepsilon^{(\ell_1,l_1)}_k \right|^2. \end{aligned} \tag{18}$$

The expression in (18) shows that the variance of $\alpha_{j,k}$ is independent of j (ie, $\sigma^2_{\alpha_{j,k}} = \sigma^2_{\alpha_k} \forall j \in [1 : 2N_{\mathrm{Rx}}]$). Therefore, the PDF of $\alpha_{j,k}$ may be expressed as:[7]

$$\mathcal{F}_{\alpha_{j,k}}\left(\alpha_{j,k}\right) = \frac{\alpha_{j,k}\left(1+q^2\right)}{q\sigma_{\alpha_k}} \exp\left(-\frac{\alpha^2_{j,k}\left(1+q^2\right)^2}{4q^2\sigma_{\alpha_k}} \right) \mathrm{I}_0\left(\frac{\alpha^2_{j,k}\left(1-q^4\right)}{4q^2\sigma_{\alpha_k}} \right), \tag{19}$$

where $\mathrm{I}_0(\cdot)$ denotes the zeroth order Bessel function of the first kind. The corresponding moment generating function (MGF) of $\alpha_{j,k}$ is given by Simon and Alouini[7] as:

$$\mathrm{M}_k(s) = \left[1 + 2s\sigma^2_{\alpha_k} + \left(\frac{2sq\sigma^2_{\alpha_k}}{1+q^2} \right)^2 \right]^{-\frac{1}{2}}, \tag{20}$$

where q is the Nakagami-q fading parameter, as defined in the system model in Section 2.3.

The PEP in (17) may then be expressed in terms of the MGF as:

$$\mathcal{P}\left(\ell_1 \to l_1\right) \approx \frac{1}{4r} \prod_{j=1}^{2N_{\mathrm{Rx}}} \mathrm{M}_1\left(\frac{1}{4}\right) \mathrm{M}_2\left(\frac{1}{4}\right) + \frac{1}{2r} \prod_{j=1}^{2N_{\mathrm{Rx}}} \sum_{R=1}^{r-1} \mathrm{M}_1\left(\frac{1}{4\sin^2\left(\frac{R\pi}{2r}\right)} \right) \mathrm{M}_2\left(\frac{1}{4\sin^2\left(\frac{R\pi}{2r}\right)} \right). \tag{21}$$

For uncorrelated channels with identical distributions, $\alpha_{j,1}$ has the same distribution for all $j \in [1 : 2N_{\mathrm{Rx}}]$. The same is true for $\alpha_{j,2}$. This is evident as the MGF is independent of j, as shown in (20). Thus, the final expression for the PEP of the STPLD system in uncorrelated Nakagami-q channels, modified from (21) and substituting (18) and (20), is:

$$\begin{aligned}\mathcal{P}\left(\ell_1 \to l_1\right) &\approx \frac{1}{4r}\left[\mathrm{M}_1\left(\frac{1}{4}\right) \mathrm{M}_2\left(\frac{1}{4}\right) \right]^{2N_{\mathrm{Rx}}} + \frac{1}{2r} \sum_{R=1}^{r-1} \left[\mathrm{M}_1\left(\frac{1}{4\sin^2\left(\frac{R\pi}{2r}\right)} \right) \mathrm{M}_2\left(\frac{1}{4\sin^2\left(\frac{R\pi}{2r}\right)} \right) \right]^{2N_{\mathrm{Rx}}} \\ &\approx \frac{1}{4r} \prod_{k=1}^{2} \left[1 + \frac{E_{\mathrm{Tx}}}{4E_\omega E_{\mathrm{n}}} \left| \varepsilon^{(\ell_1,l_1)}_k \right|^2 + \left(\frac{qE_{\mathrm{Tx}}}{4E_\omega E_{\mathrm{n}}(1+q^2)} \left| \varepsilon^{(\ell_1,l_1)}_k \right|^2 \right)^2 \right]^{-N_{\mathrm{Rx}}} \\ &\quad + \frac{1}{2r} \prod_{k=1}^{2} \sum_{R=1}^{r-1} \left[1 + \frac{E_{\mathrm{Tx}}}{4E_\omega E_{\mathrm{n}} \sin^2\left(\frac{R\pi}{2r}\right)} \left| \varepsilon^{(\ell_1,l_1)}_k \right|^2 + \left(\frac{qE_{\mathrm{Tx}} \left| \varepsilon^{(\ell_1,l_1)}_k \right|^2}{4E_\omega E_{\mathrm{n}} \left(1+q^2\right) \sin^2\left(\frac{R\pi}{2r}\right)} \right)^2 \right]^{-N_{\mathrm{Rx}}}. \end{aligned} \tag{22}$$

The final expression for the ABEP of the uncorrelated STPLD system is obtained by substituting (22) in (8). This is written in terms of the total average SNR, γ, as defined in Section 2 as:

$$\mathcal{P}_e \leq \sum_{\ell_1=0}^{M-1}\sum_{l_1=0}^{M-1}\frac{\Delta(\ell_1,l_1)}{4Mmr}\prod_{k=1}^{2}\left[1+\frac{\gamma}{4}\left|\varepsilon_k^{(\ell_1,l_1)}\right|^2+\left(\frac{q\gamma}{4(1+q^2)}\left|\varepsilon_k^{(\ell_1,l_1)}\right|^2\right)^2\right]^{-N_{\mathrm{Rx}}}$$
$$+\sum_{\ell_1=0}^{M-1}\sum_{l_1=0}^{M-1}\frac{\Delta(\ell_1,l_1)}{2Mmr}\prod_{k=1}^{2}\sum_{R=1}^{r-1}\left[1+\frac{\gamma}{4\sin^2\left(\frac{R\pi}{2r}\right)}\left|\varepsilon_k^{(\ell_1,l_1)}\right|^2+\left(\frac{q\gamma\left|\varepsilon_k^{(\ell_1,l_1)}\right|^2}{4\left(1+q^2\right)\sin^2\left(\frac{R\pi}{2r}\right)}\right)^2\right]^{-N_{\mathrm{Rx}}}. \tag{23}$$

3.2 | Correlated error performance

To analyze the error performance of the STPLD system in the presence of correlation, this article adopts the mathematical framework developed by Hedayet et al.[56] To utilize this framework, it is necessary to consider the union bound of the ABEP without making a high-SNR assumptions, as was done in Section 3.1. The union bound of the system is then given by:

$$\mathcal{P}_e \leq \frac{1}{M^2}\sum_{\ell_1=0}^{M-1}\sum_{l_1=0}^{M-1}\sum_{\ell_2=0}^{M-1}\sum_{l_2=0}^{M-1}\frac{\Delta(\ell_1,l_1)+\Delta(\ell_2,l_2)}{2m}\mathcal{P}\left([\ell_1 \quad \ell_2]^{\mathrm{T}} \rightarrow [l_1 \quad l_2]^{\mathrm{T}}\right), \tag{24}$$

where $\Delta(\ell_1,l_1)$ is the number of bit errors between ℓ_1 and l_1, as in (8). Similarly, $\Delta(\ell_2,l_2)$ is the number of bit errors between ℓ_2 and l_2. $\mathcal{P}\left([\ell_1 \quad \ell_2]^{\mathrm{T}} \rightarrow [l_1 \quad l_2]^{\mathrm{T}}\right)$ is the PEP that transmitted codeword vector $[\ell_1 \quad \ell_2]^{\mathrm{T}}$ is incorrectly detected as codeword vector $[l_1 \quad l_2]^{\mathrm{T}}$.

For correlated analysis, the PEP conditioned on perfect knowledge of all channels is given by:

$$\mathcal{P}\left([\ell_1 \quad \ell_2]^{\mathrm{T}} \rightarrow [l_1 \quad l_2]^{\mathrm{T}} \mid \mathbf{h}_{\mathrm{P1}_1}^{(1)}, \mathbf{h}_{\mathrm{P2}_1}^{(1)}, \mathbf{h}_{\mathrm{P1}_1}^{(2)}, \mathbf{h}_{\mathrm{P2}_1}^{(2)}, \mathbf{h}_{\mathrm{P1}_2}^{(1)}, \mathbf{h}_{\mathrm{P2}_2}^{(1)}, \mathbf{h}_{\mathrm{P1}_2}^{(2)}, \mathbf{h}_{\mathrm{P2}_2}^{(2)}\right)$$
$$= \mathcal{P}\left(\sum_{k=1}^{2}\left\| \sqrt{\frac{E_{\mathrm{Tx}}}{4E_\omega E_{\mathrm{n}}}}\begin{bmatrix}\mathbf{h}_{\mathrm{P1}_k}^{(1)} & \mathbf{h}_{\mathrm{P2}_k}^{(1)} & \mathbf{h}_{\mathrm{P1}_k}^{(2)} & \mathbf{h}_{\mathrm{P2}_k}^{(2)}\end{bmatrix}\begin{bmatrix}\varepsilon_k^{(\ell_1,l_1)}\\ \varepsilon_k^{(\ell_2,l_2)}\\ \varepsilon_k^{(\ell_2,l_2)}\\ \varepsilon_k^{(\ell_1,l_1)}\end{bmatrix}+\mathbf{n}_k\right\|^2 < \|\mathbf{n}_1\|^2+\|\mathbf{n}_2\|^2\right)$$
$$= \mathcal{P}\left(\sum_{k=1}^{2}\left\| \sqrt{\frac{E_{\mathrm{Tx}}}{4E_\omega E_{\mathrm{n}}}}\begin{bmatrix}\mathbf{h}_{\mathrm{P1}_k}^{(1)} & \mathbf{h}_{\mathrm{P2}_k}^{(1)} & \mathbf{h}_{\mathrm{P1}_k}^{(2)} & \mathbf{h}_{\mathrm{P2}_k}^{(2)}\end{bmatrix}\boldsymbol{\mathcal{E}}_k+\mathbf{n}_k\right\|^2 < \|\mathbf{n}_1\|^2+\|\mathbf{n}_2\|^2\right) \tag{25}$$
$$= \mathcal{P}\left(\sum_{k=1}^{2}\left\| \sqrt{\frac{E_{\mathrm{Tx}}}{4E_\omega E_{\mathrm{n}}}}\mathbf{C}_{\mathrm{Rx}}^{\frac{1}{2}}\begin{bmatrix}\hat{\mathbf{h}}_{\mathrm{P1}_k}^{(1)} & \hat{\mathbf{h}}_{\mathrm{P2}_k}^{(1)} & \hat{\mathbf{h}}_{\mathrm{P1}_k}^{(2)} & \hat{\mathbf{h}}_{\mathrm{P2}_k}^{(2)}\end{bmatrix}\left(\mathbf{C}_{\mathrm{Tx}}^{\frac{1}{2}}\right)^{\mathrm{T}}\boldsymbol{\mathcal{E}}_k+\mathbf{n}_k\right\|^2 < \|\mathbf{n}_1\|^2+\|\mathbf{n}_2\|^2\right), \tag{26}$$

where $\varepsilon_k^{\ell_k,l_k}, k \in [1:2]$, is defined in (12). In the final step, (26) is obtained by substituting the Kronecker correlation model given in (3) into (25). The difference vector, $\boldsymbol{\mathcal{E}}_k$, which was introduced in (25) is defined as:

$$\boldsymbol{\mathcal{E}}_k = \begin{bmatrix}\varepsilon_k^{(\ell_1,l_1)} & \varepsilon_k^{(\ell_2,l_2)} & \varepsilon_k^{(\ell_2,l_2)} & \varepsilon_k^{(\ell_1,l_1)}\end{bmatrix}^{\mathrm{T}}. \tag{27}$$

Substituting $\mathbf{G}_k = \sqrt{\frac{E_{\mathrm{Tx}}}{4E_\omega E_{\mathrm{n}}}}\mathbf{C}_{\mathrm{Rx}}^{\frac{1}{2}}\begin{bmatrix}\hat{\mathbf{h}}_{\mathrm{P1}_k}^{(1)} & \hat{\mathbf{h}}_{\mathrm{P2}_k}^{(1)} & \hat{\mathbf{h}}_{\mathrm{P1}_k}^{(2)} & \hat{\mathbf{h}}_{\mathrm{P2}_k}^{(2)}\end{bmatrix}\left(\mathbf{C}_{\mathrm{Tx}}^{\frac{1}{2}}\right)^{\mathrm{T}}\boldsymbol{\mathcal{E}}_k, k \in [1:2]$ in (26) and defining the amplitude $\beta_{j,k} = |G_{j,k}|$, where $G_{j,k}$ is the jth entry of $\mathbf{G}_k, j \in [1:2N_{\mathrm{Rx}}]$, the unconditioned PEP is obtained by following the same process as given by (13)–(17). The resulting expression for the unconditioned PEP is:

$$\begin{aligned}
&\mathcal{P}\left([\ell_1 \quad \ell_2]^{\mathrm{T}} \to [l_1 \quad l_2]^{\mathrm{T}}\right) \\
&\approx \frac{1}{4r}\prod_{j=1}^{2N_{\mathrm{Rx}}}\int_0^{\infty}\exp\left(-\frac{\beta_{j,1}^2}{4}\right)\mathcal{F}_{\beta_{j,1}}\left(\beta_{j,1}\right)\,\mathrm{d}\beta_{j,1}\int_0^{\infty}\exp\left(-\frac{\beta_{j,2}^2}{4}\right)\mathcal{F}_{\beta_{j,2}}\left(\beta_{j,2}\right)\,\mathrm{d}\beta_{j,2} \\
&+ \frac{1}{2r}\prod_{j=1}^{2N_{\mathrm{Rx}}}\sum_{R=1}^{r-1}\int_0^{\infty}\exp\left(-\frac{\beta_{j,1}^2}{4\sin^2\left(\frac{R\pi}{2r}\right)}\right)\mathcal{F}_{\beta_{j,1}}\left(\beta_{j,1}\right)\,\mathrm{d}\beta_{j,1}\int_0^{\infty}\exp\left(-\frac{\beta_{j,2}^2}{4\sin^2\left(\frac{R\pi}{2r}\right)}\right)\mathcal{F}_{\beta_{j,2}}\left(\beta_{j,2}\right)\,\mathrm{d}\beta_{j,2}.
\end{aligned} \tag{28}$$

As was the case in uncorrelated analysis, the random variable $\beta_{j,k}, j \in [1 : N_{\mathrm{Rx}}], k \in [1 : 2]$ follows a Nakagami-q distribution with zero mean and variance $\sigma^2_{\beta_{j,k}}$ in this study. Thus, similar to (19), the PDF of $\beta_{j,k}$ is:

$$\mathcal{F}_{\beta_{j,k}}\left(\beta_{j,k}\right) = \frac{\beta_{j,k}\left(1+q^2\right)}{q\sigma_{\beta_{j,k}}}\exp\left(-\frac{\beta_{j,k}^2\left(1+q^2\right)^2}{4q^2\sigma_{\beta_{j,k}}}\right)\mathrm{I}_0\left(\frac{\beta_{j,k}^2\left(1-q^4\right)}{4q^2\sigma_{\beta_{j,k}}}\right). \tag{29}$$

The method to calculate the variance of $\beta_{j,k}$ follows from the analytical framework formulated by Hedayet et al.[56] The starting point of this analysis is to consider the definition of $\|\mathbf{G}_k\|^2$, given by:

$$\begin{aligned}
\|\mathbf{G}_k\|^2 &= \left\|\sqrt{\frac{E_{\mathrm{Tx}}}{4E_\omega E_{\mathrm{n}}}}\mathbf{C}_{\mathrm{Rx}}^{\frac{1}{2}}\left[\hat{\mathbf{h}}_{\mathrm{P1}_k}^{(1)} \quad \hat{\mathbf{h}}_{\mathrm{P2}_k}^{(1)} \quad \hat{\mathbf{h}}_{\mathrm{P1}_k}^{(2)} \quad \hat{\mathbf{h}}_{\mathrm{P2}_k}^{(2)}\right]\left(\mathbf{C}_{\mathrm{Tx}}^{\frac{1}{2}}\right)^{\mathrm{T}}\boldsymbol{\mathcal{E}}_k\right\|^2 \\
&= \frac{E_{\mathrm{Tx}}}{4E_\omega E_{\mathrm{n}}}\mathrm{Tr}\left\{\mathbf{C}_{\mathrm{Rx}}\left[\hat{\mathbf{h}}_{\mathrm{P1}_k}^{(1)} \quad \hat{\mathbf{h}}_{\mathrm{P2}_k}^{(1)} \quad \hat{\mathbf{h}}_{\mathrm{P1}_k}^{(2)} \quad \hat{\mathbf{h}}_{\mathrm{P2}_k}^{(2)}\right]\left[\bar{\hat{\mathbf{h}}}_{\mathrm{P1}_k}^{(1)} \quad \bar{\hat{\mathbf{h}}}_{\mathrm{P2}_k}^{(1)} \quad \bar{\hat{\mathbf{h}}}_{\mathrm{P1}_k}^{(2)} \quad \bar{\hat{\mathbf{h}}}_{\mathrm{P2}_k}^{(2)}\right]^{\mathrm{T}}\mathbf{C}_{\mathrm{Tx}}\,\boldsymbol{\mathcal{E}}_k\bar{\boldsymbol{\mathcal{E}}}_k^{\mathrm{T}}\right\}.
\end{aligned} \tag{30}$$

Observing that $\mathbf{C}_{\mathrm{Rx}}$ is a full rank $2N_{\mathrm{Rx}} \times 2N_{\mathrm{Rx}}$ square matrix, it may be replaced in (30) by a $2N_{\mathrm{Rx}} \times 2N_{\mathrm{Rx}}$ diagonal matrix consisting of its $2N_{\mathrm{Rx}}$ distinct eigenvalues. These eigenvalues are denoted $V_j, j \in [1 : 2N_{\mathrm{Rx}}]$. Using a similar observation, $\mathbf{C}_{\mathrm{Tx}}\,\boldsymbol{\mathcal{E}}_k\bar{\boldsymbol{\mathcal{E}}}_k^{\mathrm{T}}$ has rank one, thus it has only one nonzero eigenvalue, denoted W_k. Thus (30) may be simplified to:

$$\|\mathbf{G}_k\|^2 = \frac{E_{\mathrm{Tx}}}{4E_\omega E_{\mathrm{n}}}\mathrm{Tr}\left\{\begin{bmatrix}|V_1| & \cdots & 0\\ 0 & \ddots & 0\\ 0 & \cdots & |V_{2N_{\mathrm{Rx}}}|\end{bmatrix}\left[\hat{\mathbf{h}}_{\mathrm{P1}_k}^{(1)} \quad \hat{\mathbf{h}}_{\mathrm{P2}_k}^{(1)} \quad \hat{\mathbf{h}}_{\mathrm{P1}_k}^{(2)} \quad \hat{\mathbf{h}}_{\mathrm{P2}_k}^{(2)}\right]\left[\bar{\hat{\mathbf{h}}}_{\mathrm{P1}_k}^{(1)} \quad \bar{\hat{\mathbf{h}}}_{\mathrm{P2}_k}^{(1)} \quad \bar{\hat{\mathbf{h}}}_{\mathrm{P1}_k}^{(2)} \quad \bar{\hat{\mathbf{h}}}_{\mathrm{P2}_k}^{(2)}\right]^{\mathrm{T}}|W_k|\right\}. \tag{31}$$

Recalling that $\beta_{j,k} = |G_{j,k}|$, the variance of $\beta_{j,k}$ is obtained by performing elementary manipulation to (31) and following a similar process to (18). The final result for the variance $\sigma^2_{\beta_{j,k}}$ is given by:

$$\sigma^2_{\beta_{j,k}} = \frac{E_{\mathrm{Tx}}}{4E_\omega E_{\mathrm{n}}}\left|V_j W_k\right|, \quad j \in [1 : 2N_{\mathrm{Rx}}], k \in [1 : 2]. \tag{32}$$

Thus, the MGF for $\beta_{j,k}$, which corresponds to the PDF given in (29), is defined as:[7]

$$\mathrm{M}_{j,k}^{\mathrm{corr.}}(s) = \left[1 + 2s\sigma^2_{\beta_{j,k}} + \left(\frac{2sq\sigma^2_{\beta_{j,k}}}{1+q^2}\right)^2\right]^{-\frac{1}{2}} = \left[1 + \frac{E_{\mathrm{Tx}}}{2E_\omega E_{\mathrm{n}}}\left|V_j W_k\right| + \left(\frac{qE_{\mathrm{Tx}}}{2E_\omega E_{\mathrm{n}}(1+q^2)}\left|V_j W_k\right|\right)^2\right]^{-\frac{1}{2}}. \tag{33}$$

Finally, the PEP of the STPLD system in the presence of correlation is given by expressing (28) in terms of the MGF of $\beta_{j,k}$, and then substituting (33). The resulting expression is given by:

$$\mathcal{P}\left([\ell_1 \quad \ell_2]^{\mathrm{T}} \to [l_1 \quad l_2]^{\mathrm{T}}\right) \approx \frac{1}{4r}\prod_{j=1}^{2N_{\mathrm{Rx}}}\prod_{k=1}^{2} \mathrm{M}_{j,k}^{\mathrm{corr.}}\left(\frac{1}{4}\right) + \frac{1}{2r}\prod_{j=1}^{2N_{\mathrm{Rx}}}\prod_{k=1}^{2}\sum_{R=1}^{r-1} \mathrm{M}_{j,k}^{\mathrm{corr.}}\left(\frac{1}{4\sin^2\left(\frac{R\pi}{2r}\right)}\right)$$
$$\approx \frac{1}{4r}\prod_{j=1}^{2N_{\mathrm{Rx}}}\prod_{k=1}^{2}\left[1 + \frac{E_{\mathrm{Tx}}}{8E_\omega E_{\mathrm{n}}}\left|V_j W_k\right| + \left(\frac{qE_{\mathrm{Tx}}}{8E_\omega E_{\mathrm{n}}(1+q^2)}\left|V_j W_k\right|\right)^2\right]^{-\frac{1}{2}}$$
$$+ \frac{1}{2r}\prod_{j=1}^{2N_{\mathrm{Rx}}}\prod_{k=1}^{2}\sum_{R=1}^{r-1}\left[1 + \frac{E_{\mathrm{Tx}}}{8E_\omega E_{\mathrm{n}}\sin^2\left(\frac{R\pi}{2r}\right)}\left|V_j W_k\right| + \left(\frac{qE_{\mathrm{Tx}}}{8E_\omega E_{\mathrm{n}}\left(1+q^2\right)\sin^2\left(\frac{R\pi}{2r}\right)}\left|V_j W_k\right|\right)^2\right]^{-\frac{1}{2}}. \quad (34)$$

The final ABEP for the correlated STPLD system is then given by substituting (34) in (24). Writing the result in terms of the total average SNR, γ, yields the expression:

$$\mathcal{P}_e \leq \sum_{\ell_1=0}^{M-1}\sum_{l_1=0}^{M-1}\sum_{\ell_2=0}^{M-1}\sum_{l_2=0}^{M-1}\frac{\Delta(\ell_1,l_1)+\Delta(\ell_2,l_2)}{8M^2mr}\prod_{j=1}^{2N_{\mathrm{Rx}}}\prod_{k=1}^{2}\left[1 + \frac{\gamma}{8}\left|V_j W_k\right| + \left(\frac{q\gamma}{8(1+q^2)}\left|V_j W_k\right|\right)^2\right]^{-\frac{1}{2}}$$
$$+ \sum_{\ell_1=0}^{M-1}\sum_{l_1=0}^{M-1}\sum_{\ell_2=0}^{M-1}\sum_{l_2=0}^{M-1}\frac{\Delta(\ell_1,l_1)+\Delta(\ell_2,l_2)}{4M^2mr}\prod_{j=1}^{2N_{\mathrm{Rx}}}\prod_{k=1}^{2}\sum_{R=1}^{r-1}\left[1 + \frac{\gamma}{8\sin^2\left(\frac{R\pi}{2r}\right)}\left|V_j W_k\right| + \left(\frac{q\gamma}{8\left(1+q^2\right)\sin^2\left(\frac{R\pi}{2r}\right)}\left|V_j W_k\right|\right)^2\right]^{-\frac{1}{2}}. \quad (35)$$

It is noted that (35) may also be used to evaluate uncorrelated STPLD systems, or STPLD systems with either transmit-side or receive-side correlation. To model a system with no transmit-side correlation, $\mathbf{C}_{\mathrm{Tx}}$ is set to a $2N_{\mathrm{Tx}} \times 2N_{\mathrm{Tx}}$ identity matrix in (26). Similarly, to model a system with no receive-side correlation, $\mathbf{C}_{\mathrm{Rx}}$ is set to a $2N_{\mathrm{Rx}} \times 2N_{\mathrm{Rx}}$ identity matrix in (26).

4 | SECONDARY MAPPER DESIGN TO ACHIEVE LABELING DIVERSITY

As described in Section 2.3, the proposed STPLD system utilizes two binary mappers, ω_1 and ω_2, to encode information codewords to constellation symbols prior to transmission. The design of ω_1 and ω_2 determines the extent to which labeling diversity is achieved in the system, influencing its error performance.

The design of mappers for labeling diversity systems is an ongoing research problem.[32-34,57-59] For a constellation with modulation order M, there are $M!$ possible designs for each mapper. Hence, there are $(M!)^2$ possible designs for the mapper pair ω_1 and ω_2. Even for a relatively low modulation order of $M = 8$, this results in a joint candidate mapper space of more than 1.62×10^9. Due to the enormity of the joint candidate mapper space, proving the optimality of a pair of mappers remains an open research problem. Recent works on labeling diversity mapper design[32-34] have focused on the case where the primary mapper is known, and only a secondary mapper needs to be designed. This follows on from the research of Samra et al,[57] which indicates that it is optimal to design the primary mapper to perform a Gray coding.

Most of the previous works on labeling diversity mapper design may be classified as either geometric designs or search-based designs. Geometric designs are able to produce secondary mappers that achieve labeling diversity for specific modulation schemes based on heuristics obtained from the geometry of constellation points.[32,33,58] The most common heuristics are obtained by considering symmetry within the constellation. There are two key drawbacks of this approach. The first drawback is that the reliance on geometric heuristics, such as symmetry, constrains the modulation schemes that may be considered. The second drawback is that the quality of the secondary mapper is dependent on the choice of heuristic used. Hence, a poorly-selected heuristic may result in a design that fails to achieve labeling diversity. Quazi and Patel[33] study this in more detail using various heuristic designs for circular and rectangular constellations in their related work.

The search-based approach to labeling diversity mapper design[34,57,59] is more generic than its geometric counterpart, however it is too computationally expensive to perform exhaustive searches through the $M!$ candidate secondary

mapper space.[57] Samra et al[57] showed that labeling diversity mapper design is an instance of the quadratic assignment problem (QAP), and utilized a branch-and-bound QAP-solver[60] to produce labeling diversity mappers. The QAP-solver produces an optimal labeling diversity secondary mapper for modulation orders $M \leq 16$, as stated by Samra et al[57] and verified by Xu et al.[32] However, the computational cost of the QAP solver made this approach unsuitable for modulation orders.[57] A recent work in labeling diversity mapper design by Patel et al[34] utilized a genetic algorithm (GA) to develop secondary mappers for USTLD systems. The GA performs a heuristic search through the candidate mapper space, and is thus unconstrained by possible asymmetry of constellation points. It was also shown by Patel et al[34] that the use of a GA is computationally feasible for modulation orders $M > 16$. Therefore, in this article, the GA proposed by Patel et al[34] is modified and applied to design secondary mappers that achieve labeling diversity for STPLD systems. The modification is based on the two-stage approach to evaluating and comparing candidate secondary mapper designs in recent literature,[33] and this is detailed in Section 4.2.1.

4.1 | High level description of genetic algorithm for secondary mapper design

Figure 2 provides a high-level illustration of the genetic algorithm for labeling diversity mapper design used in this article. Candidate secondary mappers are encoded into data structures called "chromosomes," which consists of sub-units referred to as "genes." The notation used in this section is to represent genes and chromosomes by variables x and $\boldsymbol{\mathcal{X}}$. Each chromosome consists of M genes, $x_i, i \in [1 : M]$, each of which correspond to a symbol from the M-ary constellation. The value contained within each gene of the chromosome is the label associated with that constellation point. Hence the chromosome is defined as $\boldsymbol{\mathcal{X}} = \begin{bmatrix} x_1 & x_2 & \cdots & x_{M-1} & x_M \end{bmatrix}$ and fully describes a candidate secondary mapper. The set of candidate secondary mappers (ie, chromosomes) considered at in each iteration of the GA is referred to as the "population," and the size of the population is denoted as S. In terms of notation, $\{\boldsymbol{\mathcal{X}}\}^{(n)}$ denotes the population at iteration n. $\{\boldsymbol{\mathcal{X}}\}^{(0)}$ is set up according to the initial population configuration approach described by Patel et al.[34]

During each iteration, the population is modified to model the biological processes of "mating," "evolution," and "natural selection." "Parent" chromosomes from within the population "mate" to produce "child" chromosomes, which are added to the population. This algorithmic process is referred to as "crossover."

The design of the crossover algorithm ensures that desirable properties from the parent chromosomes are passed on to the child chromosomes. To design labeling diversity mappers, Patel et al[34] developed a new crossover technique called the $\mathcal{K}$-point hypersphere swap crossover ($\mathcal{K}$-HSX). In the $\mathcal{K}$-HSX, the genes to be swapped at each iteration are chosen such that they fall outside a hypersphere with the 4-dimensional hyperspace defined by the constellation representation of the two parent chromosomes. This ensures that the genes will have different neighbors in the hyperspace after swapping. In other words, the distances between the genes that were swapped and their hyperspace neighbors are greater in the child chromosomes than in the parent chromosomes. The reader is referred to Section III-B2 of the original work[34] for full details of the $\mathcal{K}$-HSX, including a procedural example of the swapping process.

When mimicking evolution, the algorithmic process of the GA is referred to as "mutation." Mutation is a random event that occurs when a child chromosome undergoes further changes after crossover. The probability of a mutation

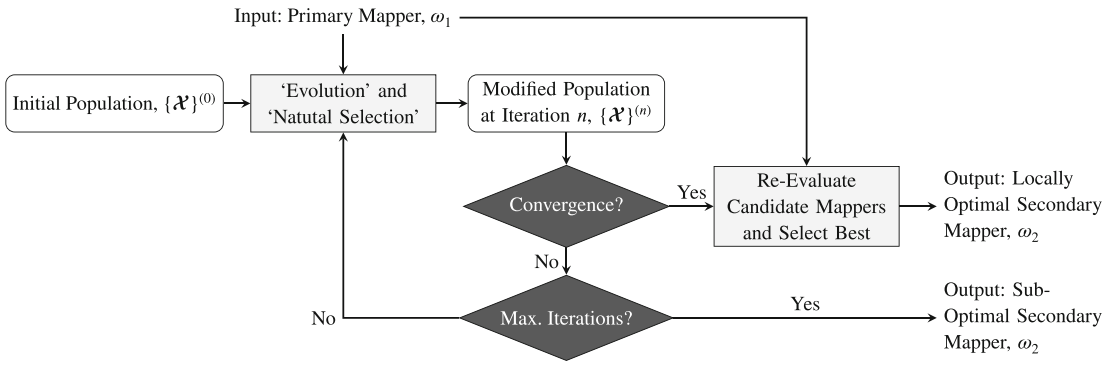

FIGURE 2 High-level illustration of genetic algorithm

occurring for a given child chromosome is denoted $\mathcal{P}_m$. This work applies the same mutation algorithm as described by Patel et al.[34]

After crossover and mutation, the population of candidate secondary mappers is greater than the initial population. Natural selection is then mimicked by pruning the population to maintain only the best candidate secondary mappers. This is done by evaluating the entire population using a "fitness function," which requires knowledge of the primary mapper, ω_1, as described by Patel et al.[34] After evaluating the fitness of chromosomes within the population, the least-fit chromosomes are removed. In this article, the fitness of chromosome $\boldsymbol{\mathcal{X}}$ is denoted $\varphi(\boldsymbol{\mathcal{X}})$. The output of the "evolution" and "natural selection" processes is a modified population at each iteration of the GA.

The GA stops iterating when chromosomes within the population have converged to the same fitness score. If the GA converges, it determines that a locally optimal (but not necessarily globally optimal) candidate mapper exists within the population. All chromosomes in the population are then re-evaluated using a "selection function," which also requires knowledge of ω_1, to identify the locally optimal mapper. The locally optimal mapper is then selected as the output of the GA. The use of the selection function to select the locally optimal mapper from within the converged population is the key difference between the modified GA utilized in this article and its previous variant.[34]

To ensure that the GA is not computationally intractable, an upper bound on the number of iterations that may be performed is set. This is denoted $n_{\max}$. Patel et al[34] discuss that selecting $n_{\max} \ll M^5$ ensures that the GA is less computationally expensive than the branch-and-bound QAP-solver used by Samra et al.[57] If the GA reaches the maximum number of iterations without converging, then the candidate secondary mapper corresponding to the fittest chromosome (as determined by the fitness function) in the population is selected as the output of the GA. In this case, the output is classified as sub-optimal. Hence, there are two conditions under which the GA will terminate: (i) a locally optimal solution has been reached and further iterations do not improve the fitness of the population, or (ii) the maximum bound on the number of iterations has been reached.

In this work, the authors have enhanced the evaluation of candidate secondary mappers during the natural selection process and the final evaluation of chromosomes during termination. This is based on the latest approach to labeling diversity mapper analysis,[33] and is described in more detail in the following subsection.

4.2 | Novel modifications to the genetic algorithm for labeling diversity mapper design

As mentioned in the previous subsection, the genetic algorithm developed for designing labeling diversity mappers evaluates chromosomes within the candidate mapper population at two points: (i) when imitating "natural selection" and (ii) when selecting the locally optimal candidate mapper from the converged population during "termination." During "natural selection," all chromosomes are evaluated using the fitness function. If the population converges, all chromosomes have the same fitness. Thus, further iterations of the mating process are unlikely to improve the fitness of chromosomes within the population, and the GA terminates its iterative search. To select the best chromosome from within this converged population, a different metric is required. This metric is computed using the selection function.

The remainder of this subsection focuses on developing the mathematical framework for evaluating candidate secondary mappers, based on recent literature on labeling diversity mapper design.[33] Thereafter, the application of this framework to design the fitness and selection functions in the GA are discussed.

4.2.1 | Developing the mathematical framework for evaluating candidate secondary mappers

The genetic algorithm requires an analytical means to compare candidate secondary mappers, and thereby predict the extent to which each mapper achieves labeling diversity. As shown in previous literature,[32-34] the mathematical framework for comparing candidate secondary mappers is developed by taking a high-SNR approximation of the ABEP. Using (20), it is observed that as $\gamma \to \infty$, the third term of the MGF dominates. Thus, (15) at high-SNR may be approximated as:

$$\mathcal{P}(\ell_1 \to l_1) \approx \frac{1}{4r}\prod_{k=1}^{2}\left(\frac{q\gamma}{4(1+q^2)}\left|\varepsilon_k^{(\ell_1,l_1)}\right|^2\right)^{-2N_{\mathrm{Rx}}} + \frac{1}{2r}\prod_{k=1}^{2}\sum_{R=1}^{r-1}\left(\frac{q\gamma\left|\varepsilon_k^{(\ell_1,l_1)}\right|^2}{4\left(1+q^2\right)\sin^2\left(\frac{R\pi}{2r}\right)}\right)^{-2N_{\mathrm{Rx}}} \tag{36}$$

$$\approx \frac{1}{4r}\left[\left(\frac{q\gamma}{4(1+q^2)}\right)^2\left|\varepsilon_1^{(\ell_1,l_1)}\right|^2\left|\varepsilon_2^{(\ell_1,l_1)}\right|^2\right]^{-2N_{\mathrm{Rx}}} + \frac{1}{2r}\sum_{R=1}^{r-1}\left[\left(\frac{q\gamma}{4\left(1+q^2\right)\sin^2\left(\frac{R\pi}{2r}\right)}\right)^2\left|\varepsilon_1^{(\ell_1,l_1)}\right|^2\left|\varepsilon_2^{(\ell_1,l_1)}\right|^2\right]^{-2N_{\mathrm{Rx}}}. \tag{37}$$

The expression in (37) indicates that lower values of the product distance $\left|\varepsilon_1^{(\ell_1,l_1)}\right|\left|\varepsilon_2^{(\ell_1,l_1)}\right|$ result in better error performance. Using this reasoning and substituting (37) into (8), it is evident that the error floor of the ABEP is set by the minimum product distance. Thus, the objective of secondary mapper design can be formulated as the optimization problem given by:[32,33]

$$\omega_2^{\text{optimal}} = \underset{\substack{\ell_1,l_1\in[0:M-1]\\ \ell_1\neq l_1}}{\operatorname{argmax}}\ \aleph(\ell_1,l_1), \tag{38}$$

where $\aleph$ is the mapper design metric.

Based on the work by Quazi and Patel,[33] the expression in (37) gives rise to four metrics that may be used for comparing labeling diversity mappers: the minimum product distance ($\aleph_1$), the minimum summed product distance ($\aleph_2$), the minimum bit-difference-weighted product distance ($\aleph_3$) and the minimum summed bit-difference-weighted product distance ($\aleph_4$). These metrics are defined mathematically as:

$$\aleph_1 = \min_{\substack{\ell_1,l_1\in[0:M-1]\\ \ell_1\neq l_1}}\left|\varepsilon_1^{(\ell_1,l_1)}\right|\left|\varepsilon_2^{(\ell_1,l_1)}\right|, \tag{39}$$

$$\aleph_2 = \min_{\ell_1\in[0:M-1]}\sum_{l_1=0}^{M-1}\left|\varepsilon_1^{(\ell_1,l_1)}\right|\left|\varepsilon_2^{(\ell_1,l_1)}\right|, \tag{40}$$

$$\aleph_3 = \min_{\substack{\ell_1,l_1\in[0:M-1]\\ \ell_1\neq l_1}}\frac{1}{\Delta(\ell_1,l_1)}\left|\varepsilon_1^{(\ell_1,l_1)}\right|\left|\varepsilon_2^{(\ell_1,l_1)}\right|, \tag{41}$$

$$\aleph_4 = \min_{\ell_1\in[0:M-1]}\sum_{l_1=0}^{M-1}\frac{1}{\Delta(\ell_1,l_1)}\left|\varepsilon_1^{(\ell_1,l_1)}\right|\left|\varepsilon_2^{(\ell_1,l_1)}\right|. \tag{42}$$

The discussion presented by Quazi and Patel[33] shows that the most feasible approach to evaluating candidate secondary mappers is to use a 2-stage approach, considering $\aleph_1$ and $\aleph_2$. In the first stage, candidate secondary mappers are evaluated using $\aleph_1$. A larger value of $\aleph_1$ indicates a more-optimal mapper. It is possible that when evaluating the candidate secondary mappers, multiple candidates may have the same value of $\aleph_1$.[33] In this scenario, a second stage is needed to further distinguish these candidate mappers, and do this, $\aleph_2$ is used. Once again, larger values of $\aleph_2$ indicate more-optimal mappers in this case.

4.2.2 | Application of mathematical framework for evaluating candidate secondary mappers

As the genetic algorithm evaluates the population of candidate secondary mappers at two points, the 2-stage approach to mapper evaluation is straightforward to apply. When performing "natural selection," the fitness function assigns a value for $\aleph_1$ to each candidate secondary mapper. This value is used to evaluate the candidate mappers. Thus, if the population converges, all chromosomes have the same value of $\aleph_1$ and should be re-evaluated to determine $\aleph_2$. $\aleph_2$ is then used to select the locally optimum candidate mapper.

Further details on imitating "natural selection"

The biological process of "natural selection" is modeled by pruning the population of candidate secondary mappers at the end of each iteration. This is accomplished by determining the fitness of each chromosome, and discarding the least-fit chromosomes from the population. As discussed by Patel et al,[34] the mating processes of crossover and mutation result in $2\binom{S}{2}$ child chromosomes being added to the population. To ensure that the population size at the start of each iteration remains fixed, the $2\binom{S}{2}$ least-fit candidates are discarded from the population at the end of each iteration. This pruning process has 2 key benefits for the GA:

1. The number of crossovers performed at the next iteration remains constant. Since all possible pairs of parents are crossed over at each iteration, a growth in the population would result in the number of crossovers performed exponentially increasing. This would severely impact the runtime and computational tractability of the genetic algorithm.
2. By discarding the least-fit chromosomes, at the next iteration, there are fitter parent chromosomes to be crossed over. Since child chromosomes inherit desirable properties from their parents, this ensures that the population gets progressively fitter at each iteration.

As mentioned previously, the fitness of chromosomes is determined by (39) when pruning the population. Thus, after modeling "natural selection," the S chromosomes with the highest fitness form the modified population for the next iteration of the GA.

Convergence and termination

As shown in Figure 2 and discussed previously, there are two conditions under which the GA terminates. The first condition occurs when all chromosomes within the population converge to the same fitness score, which indicates that there exists a locally optimal candidate secondary mapper within the population. If this occurs, the selection function is used to compute $\aleph_2$ (which was defined in (40)). The output of the GA is then the chromosome from the converged population with the highest value of $\aleph_2$.

The second termination condition which may occur is that the GA reaches the maximum number of permitted iterations, $n_{\max}$. As suggested by Patel et al,[34] to ensure that it is computationally tractable, this parameter is chosen such that $n_{\max} \ll M^5$. If the maximum number of iterations is reached, it is assumed that the genetic algorithm will not converge. In this case, the fittest chromosome from the population, in terms of $\aleph_1$, is selected as the output.

4.3 | Designed mappers for STPLD system

The genetic algorithm for labeling diversity mapper design described in Section 4.1 was implemented to produce secondary mappers for the APSK constellations considered in this article (detailed in Table 2, Section 2). These are constellations selected from the DVB-S2X standard.[42] The constellations are shown in Figure 3, and the GA parameters used to design each mapper are detailed in Table 3. For readability, Figure 3 indicates binary labels by their decimal equivalent values. The value located below each constellation point indicates label obtained by using mapper ω_1. Similarly, the value located above each constellation point indicates the label obtained by using mapper ω_2, which was produced by the GA.

TABLE 3 Details of parameters used in implementing genetic algorithm

M	S	$\mathcal{P}_m$	$n_{\max}$	$\mathcal{K}$	Hypersphere radius for $\mathcal{K}$-HSX	Convergence reached
8	7	3%	200	3	1	Yes
16	16	8%	10^4	3	1	Yes
32	12	12%	10^5	8	5	No
64	10	15%	10^7	9	7	Yes

Note: M, modulation order; S, population size; $\mathcal{P}_m$, mutation probability; $n_{\max}$, max. iterations; $\mathcal{K}$, number of crossovers; $\mathcal{K}$-HSX, $\mathcal{K}$-point hypersphere swap crossover.[34]

5 | RESULTS AND DISCUSSION

5.1 | Error performance of proposed system

The first study of the proposed STPLD system compares its error performance to other recent MIMO schemes. To ensure a fair comparison, the study is constrained to uncoded systems. Each set of curves shows both the theoretical BER performance of all systems considered, as well as results obtained through the use of Monte Carlo simulations. All systems are assumed to be uncorrelated and subjected to fast-fading. The systems compared to STPLD are:

1. The orthogonal space-time block code (OSTBC) proposed by Alamouti[27] for terrestrial systems. This was extended to the satellite broadcasting context by Arti and Jindal[28] and Arapoglou et al.[20]
2. The orthogonal space-time-polarization block code (OSTPBC) proposed by Wysocki and Wysocki[29] for terrestrial systems. This was extended to the satellite broadcasting context by Vineetha and Kirthiga[30] and Aparna et al.[31]
3. The USTLD system proposed by Xu et al[32] for terrestrial systems. This was extended to the satellite broadcasting context by Quazi and Patel.[33]

To achieve labeling diversity, both the STPLD and USTLD systems utilize the APSK constellation mappings illustrated in Figure 3.

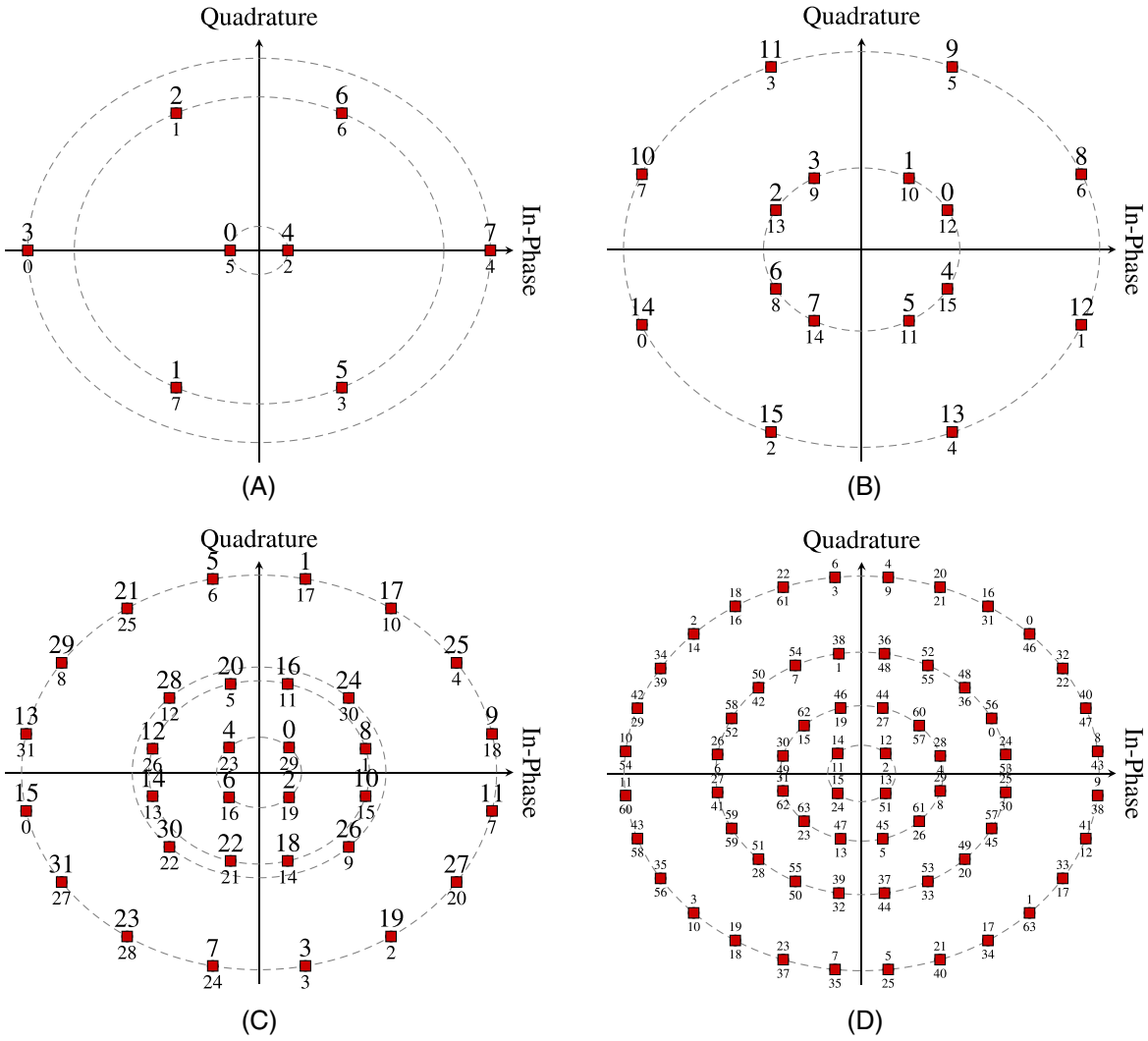

FIGURE 3 APSK constellation mappings for labeling diversity. (A) 8APSK, (B) 16APSK, (C) 32APSK, and (D) 64APSK

The results of the BER performance study are shown in Figure 4. The theoretical BER performance curves presented for the OSTBC and USTLD systems are based on analytical expressions which can be found in literature.[27,32,38] For the STPLD system, theoretical results are obtained from (23). A theoretical expression for the BER performance of the OSTPBC is not explicitly shown in literature,[29-31] however one can be obtained from (23) by exploiting the similarity in the structure of the STPLD and OSTPBC systems. This is accomplished by setting $\omega_1 = \omega_2$ in (12) and substituting the result back into (23). Since (23) was derived using the union bound, it presents an upper-bound approximation for the BER of the STPLD system which is expected to be accurate at high SNRs and inaccurate at low SNRs. The overlapping of the theoretical and simulated curves for both the STPLD and OSTPBC systems in the high-SNR region indicate that the analytical expression is a valid upper-bound and accurate at high SNRs.

As both the USTLD[32] and OSTPBC[29] systems were developed as improvements to the OSTBC[27] system, it is expected that they exhibit better error performance. This is confirmed by the results in Figure 4. Quantitatively, at a BER of 10^{-6}, the USTLD scheme improves upon the OSTBC scheme by ≈7 dB for the 2×2 16APSK system, and by ≈5 dB for both the 2×4 32APSK and 2×2 64APSK systems. This confirms that the secondary mappers produced by the genetic algorithm in Section 4 achieve a significant level of labeling diversity.

For the 16APSK and 32APSK systems, the OSTPBC scheme shows a marginal improvement of <1 dB when compared to the USTLD scheme. However, for the 64APSK system, the OSTPBC scheme improves upon the USTLD scheme by ≈2 dB. The reason for the OSTPBC scheme out-performing the USTLD scheme is attributed to its diversity. Qualitatively, diversity is indicated by the slope of the BER curves in the high-SNR region. For all three systems presented in Figure 4, the OSTPBC has a steeper gradient in the high-SNR region, and hence it achieves more diversity. To quantify this observation, the diversity order (defined in (43)) is used. It can be shown that $\Gamma_{\text{OSTPBC}} = 4N_{\text{Rx}}$, whereas $\Gamma_{\text{USTLD}} = \Gamma_{\text{OSTBC}} = 2N_{\text{Rx}}$.

$$\Gamma = -\lim_{\gamma \to \infty} \frac{\log \mathcal{P}_e(\gamma)}{\log \gamma}. \tag{43}$$

The proposed STPLD scheme incorporates the benefits of both labeling and polarization diversity, and exhibits the best error performance in all systems considered. Using (43), it can be shown that the diversity order of the STPLD system is the same as that of the OSTPBC (ie, $\Gamma_{\text{STPLD}} = \Gamma_{\text{OSTPBC}} = 4N_{\text{Rx}}$). It is also observed that the relative improvement of the STPLD scheme over the OSTPBC scheme is the same as the relative improvement of the USTLD system over the OSTBC scheme at a BER of 10^{-6}.

5.2 | Correlation study

Figure 5 shows that the analytical bound for the STPLD system presented in (35) converges to results obtained by Monte Carlo simulations. Results are presented for a 2×3 8APSK system assuming the correlation models discussed in Section 2.4. The IAI and IBI correlation coefficients at both the transmit-side and receive-side were assumed equal, such that $\rho_{\text{Tx}}^{\text{IAI}} = \rho_{\text{Rx}}^{\text{IAI}} = \rho_{\text{Tx}}^{\text{IBI}} = \rho_{\text{Rx}}^{\text{IBI}} = 0.6$. The chosen value for the correlation coefficient ensured that results differ significantly from the uncorrelated case, while also differing from the most extreme, fully-correlated case.

Qualitative inspection of the results in Figure 5A shows that the STPLD system configuration with only transmit-side correlation (Tx corr) performs worse than the system subjected to only receive-side correlation (Rx corr). Thus, it is deduced that STPLD systems are more sensitive to correlation at the transmitter than at the receiver. This is in agreement with the findings of other studies on labeling diversity systems, and has been previously explained mathematically by Patel et al.[38]

Figure 5B shows that the analytical model for the correlated STPLD system is valid for systems subject to IAI, IBI, and both IAI and IBI. The next study further investigates IAI and IBI to determine which causes a greater degradation in error performance. The analytical results of this study are presented in Figure 6. The shading of the surfaces in Figure 6 corresponds to the BER of the curve.

Figure 6A shows the effect of transmit-side IAI and IBI on an STPLD system, assuming no receive-side correlation. The symmetry of the surface plot indicates that error performance of the system is equally susceptible to both IAI and IBI. It is also observed that at low correlation coefficients, the BER performance does not noticeably degrade, as shown by the flat region of the surface with dark shading. However, once the correlation coefficients fall outside the

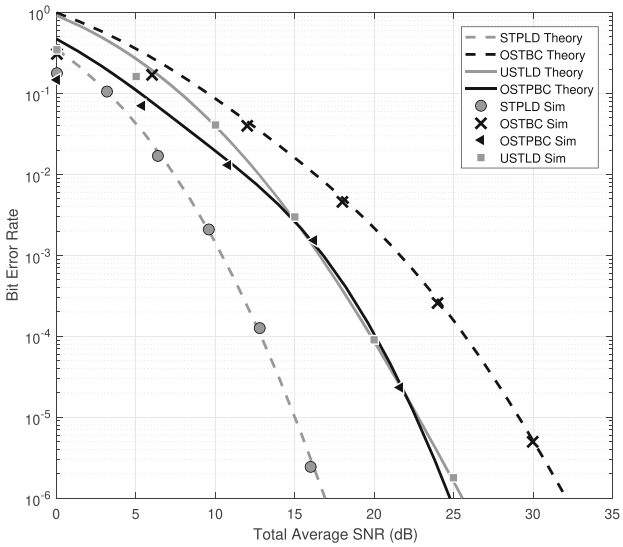

(A)

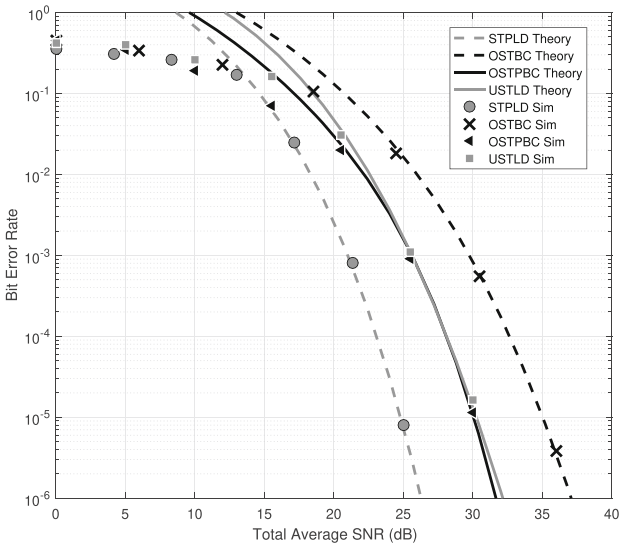

(B)

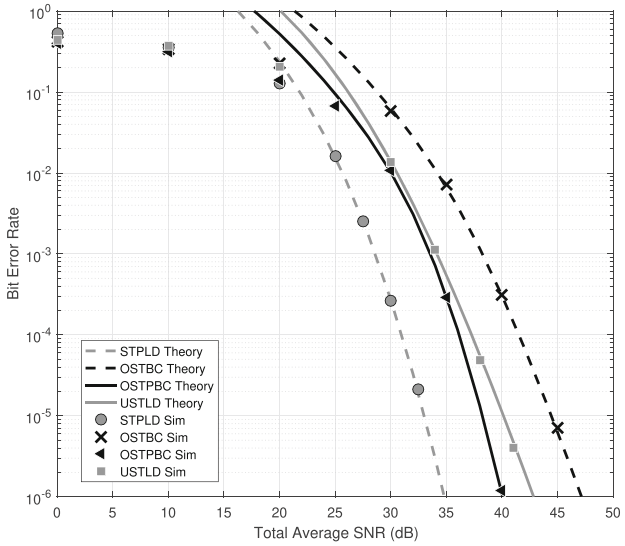

(C)

Sub-figure	N_{Tx}	N_{Rx}	Modulation Scheme	q
(a)	2	2	16APSK	0.3
(b)	2	4	32APSK	0.3
(c)	2	2	64APSK	0.7

(D)

FIGURE 4 Comparing the BER of STPLD systems with similar MIMO schemes. (A) 2×2 16APSK, $q = 0.3$, (B) 2×4 32APSK, $q = 0.3$, (C) 2×2 64APSK, $q = 0.7$, and (D) simulation parameters

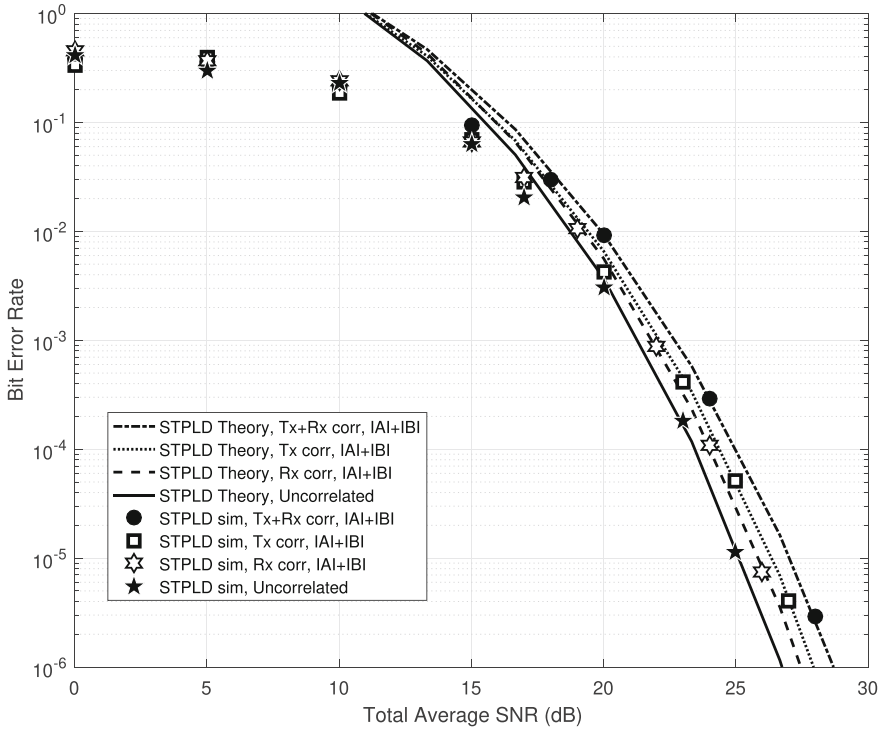

FIGURE 5 Validation of the analytical expression for the ABEP of correlated STPLD systems (given by (35)). (A) 2×3 8APSK, $q = 0.5$, transmit-side and receive-side correlation, and (B) 2×3 8APSK, $q = 0.5$, inter-antenna and inter-beam interference

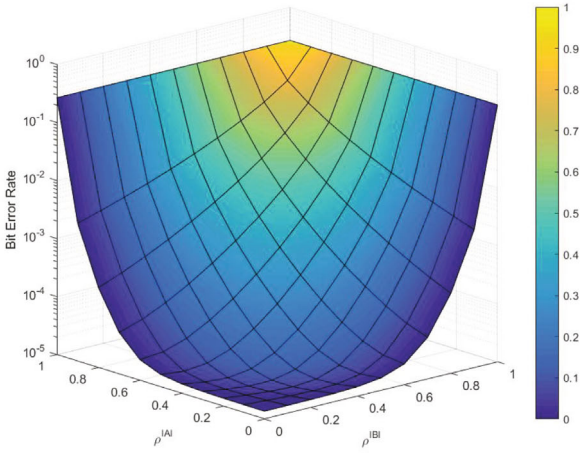

(A)

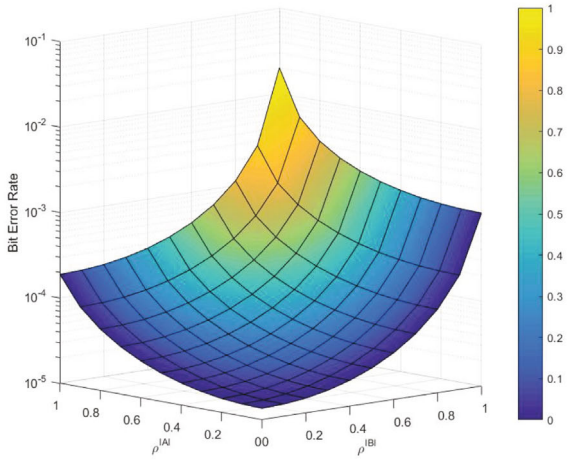

(B)

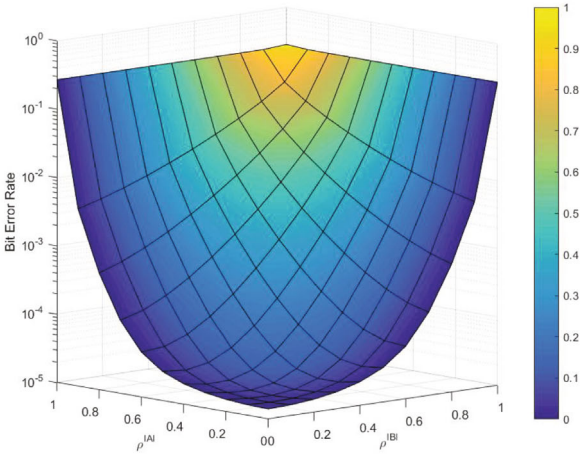

(C)

FIGURE 6 Comparing the effects of inter-antenna interference and inter-beam interference. (A) 2×3 8APSK, $q = 0.5$, $\gamma = 25$ dB, transmit-side correlation, (B) 2×3 8APSK, $q = 0.5$, $\gamma = 25$ dB, receive-side correlation, and (C) 2×3 8APSK, $q = 0.5$, $\gamma = 25$ dB, transmit-side and receive-side correlation

bounds of this region, the BER performance rapidly degrades. The worst-case performance of the STPLD system with transmit-side correlation is 4 orders of magnitude worse than the uncorrelated STPLD system. Figure 6B presents a similar set of results for receive-side correlation. By observing the contours on the surface, it is evident that as the BER performance of the system degrades more rapidly as the IBI correlation coefficient increases than as the IAI correlation coefficient increases (ie, $\frac{\partial \mathcal{P}_e}{\partial \rho^{\mathrm{IAI}}} < \frac{\partial \mathcal{P}_e}{\partial \rho^{\mathrm{IBI}}}$). This indicates that the STPLD system is more sensitive to IBI than IAI at the receiver.

Finally, Figure 6C shows the effect of IAI and IBI on an STPLD system with both transmit-side and receive-side correlation. For simplicity, it is assumed that $\rho_{\mathrm{Tx}}^{\mathrm{IAI}} = \rho_{\mathrm{Rx}}^{\mathrm{IAI}} = \rho^{\mathrm{IAI}}$ and $\rho_{\mathrm{Tx}}^{\mathrm{IBI}} = \rho_{\mathrm{Rx}}^{\mathrm{IBI}} = \rho^{\mathrm{IBI}}$. The resulting surface plot closely resembles that shown in Figure 6A. Comparing Figure 6A,C, it is observed that the contours along the surface of Figure 6C are steeper than in Figure 6A. This observation reaffirms that transmit-side correlation has a more dominant impact on error performance than receive-side correlation. It is also noted that the flat, dark-shaded region in Figure 6c extends until $\rho^{\mathrm{IBI}} \approx 0.4$ when $\rho^{\mathrm{IAI}} = 0$ and until $\rho^{\mathrm{IAI}} \approx 0.45$ when $\rho^{\mathrm{IBI}} = 0$. Thus, the surface plot presented in Figure 6C is slightly asymmetric. This indicates that when there is correlation at both the transmit-side and receive-side, the STPLD system is marginally more susceptible to IBI than IAI. This is expected, given the trends observed for only receive-side correlation discussed previously.

6 | CONCLUSION

This article proposes a terrestrial MIMO broadcasting system that achieves space, time, polarization, and labeling diversity. The proposed STPLD system is modeled under both ideal (uncorrelated) and practical (correlated) conditions. The correlation model provided allows inter-antenna and inter-beam interference to be considered at both the transmitting node and the receiving node. Analytical expressions for both correlated and uncorrelated STPLD systems are derived and corroborated by Monte Carlo simulations. The results presented assumed the Nakagami-q fading model, which gives insight into the worst-case error performance of terrestrial links.

The design of a secondary mapper to achieve labeling diversity is important to the STPLD system. To design secondary mappers for the constellations considered in this article, the latest GA for labeling diversity mapper design was modified and enhanced. This GA is applicable to any generic constellation, and in this article, it is applied to 8APSK, 16APSK, 32APSK, and 64APSK constellations. These constellations and their recommended primary mappings are taken from the DVB-S2X standard.[42]

Two studies of the STPLD system are presented. In the first study, it is found that STPLD systems achieve a diversity order of $\Gamma_{\mathrm{STPLD}} = 4N_{\mathrm{Rx}}$. Additionally, the results presented indicate the STPLD system improves performance by ≈7 dB for the 2×2 16APSK system configuration, and by ≈5 dB for both the 2×4 32APSK and 2×2 64APSK system configurations studied, when compared to the best comparable MIMO scheme (the OSTPBC). The second study of the STPLD system analyses the effects of correlation on BER performance. It is found that STPLD systems are most sensitive to correlation at the transmitter. It is also observed that at the receiver, IBI has a more dominant effect on system performance than IAI. These trends were observed when considering a 2×3 8APSK STPLD system configuration.

Future works may consider improving the spectral efficiency of the terrestrial STPLD system, as well as studying STPLD in the satellite context. For satellite broadcasting, spectral efficiency enhancement is important due to the large distances between base stations and satellites that result in high system latency—which increases in severity when transmitting the same information over multiple time slots. It is noted that this problem is common to the OSTBC, OSTPBC and USTLD systems that have previously been adapted for satellite broadcasting.[20,30,31,33] The satellite variant of the STPLD system should also consider more realistic satellite channel models, such as the hybrid model proposed by Hazra and Mitra.[61] Another relevant topic of interest is to implement the proposed system in a test-bed application.

NOMENCLATURE

N	number of antennas
ω	bit-to-symbol mapper
ℓ	information codeword
q	Nakagami-q fading parameter
M	modulation order
P1, P2	polarization 1, polarization 2

E	energy
γ	signal-to-noise ratio
$\mathbf{y}$	received signal vector
$\mathbf{h}$	vector of narrowband multipath fading coefficients
$\mathbf{C}$	correlation matrix
$\grave{\mathbf{h}}$	vector of virtual, uncorrelated multipath fading coefficients used in mathematical analysis when $\mathbf{h}$ is correlated
ρ	correlation coefficient
$\mathcal{P}(\cdot)$	probability
$\Delta(a, b)$	number of bit errors between a and b
$\mathbf{n}$	vector of AWGN terms
ε	distance between constellation points
$Q(\cdot)$	Gaussian Q-function
α	amplitude of fading
σ^2	variance
$\mathtt{M}(\cdot)$	moment generating function
V	eigenvalue of the receive-side correlation matrix
W	eigenvalue of the transmit-side correlation matrix
$\boldsymbol{\mathcal{X}}$	genetic algorithm chromosome
x	genetic algorithm gene
$\{\boldsymbol{\mathcal{X}}\}$	genetic algorithm population
S	genetic algorithm population size
$\varphi(\cdot)$	genetic algorithm fitness function
$n_{\max}$	maximum number of permissible iterations of the genetic algorithm
$\aleph$	labeling diversity mapper design metric
Γ	diversity order

FUNDING INFORMATION

All funding to support this research was provided by the University of KwaZulu-Natal and the Durban University of Technology.

CONFLICT OF INTEREST

The authors declare that there are no conflicts of interest to be disclosed with relation to this research.

DATA AVAILABILITY STATEMENT

Data sharing is not applicable to this article as no datasets were generated or analyzed during the current study.

ORCID

Sulaiman Saleem Patel https://orcid.org/0000-0003-3557-3645
Tahmid Quazi https://orcid.org/0000-0002-1288-4224

REFERENCES

1. Mietzner J, Schober R, Lampe L, Gerstacker WH, Hoeher PA. Multiple-antenna techniques for wireless communications - a comprehensive literature survey. *IEEE Commun Surv Tutor*. 2009;11(2):87-105. doi:10.1109/SURV.2009.090207
2. Goldsmith A. *Wireless Communications*. Cambridge: Cambridge University Press; 2005. doi:10.1017/CBO9780511841224
3. Saeed A, Quazi T, Xu H. Hierarchical modulated QAM with signal space diversity and MRC reception in Nakagami-m fading channels. *IET Commun*. 2013;7(12):1296-1303.
4. Saeed A, Quazi T, Xu H. Alamouti space-time block coded hierarchical modulation with signal space diversity and MRC reception in Nakagami-m fading channel. *IET Commun*. 2014;8(4):516-524.
5. Quazi T, Xu H. SSD-enhanced uncoded space-time labeling diversity. *Int J Commun Syst*. 2018;31(11):e3592. doi:10.1002/dac.3592
6. Zhang H, Dai H, Zhou Q, Hughes BL. On the diversity order of spatial multiplexing systems with transmit antenna selection: a geometrical approach. *IEEE Trans Inf Theory*. 2006;52(12):5297-5311.
7. Simon MK, Alouini M-S. *Digital Communication Over Fading Channels: A Unified Approach to Performance Analysis*. New York: John Wiley & Sons, Inc.; 2000.

8. Roztocki N, Weistroffer R. Conceptualizing and researching the adoption of ICT and the impact on socioeconomic development. *Inf Technol Dev*. 2016;22(4):541-549.
9. Cabral A, Moodley L, Yeboah-Amankwah S. Digital divide: the impact of closing Africa's internet gap. [Online Report]; 2018; McKinsey & Company. https://www.mckinsey.com/business-functions/marketing-and-sales/our-insights/digital-divide-the-impact-of-closing-africas-internet-gap. Accessed August 5, 2018.
10. Ray PK, Ray S. Resource-constrained innovation for emerging economies: the case of the indian telecommunications industry. *IEEE Trans Eng Management*. 2009;57(1):144-156.
11. Scheerder A, van Deursen A, van Dijk J. Determinants of Internet skills, uses and outcomes. A systematic review of the second- and third-level digital divide. *Telematics Inform*. 2017;34:1607-1624.
12. The United Nations General Assembly. Transforming our world: the 2030 agenda for sustainable development. [Online Report] A/RES/70/1; 2015. http://www.un.org/ga/search/view_doc.asp?symbol=A/RES/70/1&Lang=E. Accessed August 5, 2018.
13. Conte R. Satellite rural communications: telephony and narrowband networks. *Int J Satell Commun Netw*. 2005;23(5):307-321.
14. Iqbal MK, Iqbal MB, Shamoon S, Bhatti M. Future of satellite broadband Internet services and comparison with terrestrial access methods e.g. DSL and cable modem. Proceedings of the 3rd IEEE International Conference on Computer, Control and Communication; 2013:1-5; Karachi (Pakistan).
15. Yesufu AK. Possible use of satellites in rural telecommunications in Africa. Proceedings of the 2nd International Conference on Rural Telecommunication; 1990:156-159; London (England).
16. Tomassini D, Ginati A, Feliciani F, Deconick F, Gaudiano V, Cuccarese F, Recchia F, Bove A, Cabanas F, Mathee B, Halloway L, Richardson P, Francis I. Space4edu: satellite technology for smart rural schools in South Africa. Proceedings of the 64th International Astronautical Congress; 2013:4472-4479; Beijing (China).
17. Olla P. Exploiting satellite radio technology to create an African satellite health education infrastructure. Proceedings of the 57th International Astronautical Congress; 2006:8955-8961; Valencia (Spain).
18. Martín-de-Mercado G, Horsch A, Parentela G, Mancini P, Ginati A. Satellite-enhanced telemedicine and eHealth for Sub-Saharan Africa: a development opportunity. Proceedings of the 62nd International Astronautical Congress; 2011:4320-4327; Cape Town (South Africa).
19. Kyröläinen J, Hulkkonen A, Ylitalo J, et al. Applicability of MIMO to satellite communications. *Int J Satell Commun Netw*. 2014;32:343-357.
20. Arapoglou P-D, Burzigotti P, Bertinelli M, Bolea Alamanac A, De Gaudenzi R. To MIMO or not to MIMO in mobile satellite broadcasting systems. *IEEE Trans Wirel Commun*. 2011;10(9):2807-2811.
21. Arapoglou P-D, Liolis K, Bertinelli M, Panagopoulos A, Cottis P, De Gaudenzi R. MIMO over satellite: a review. *IEEE Commun Surv Tutor*. 2011;13(1):27-51.
22. Schwartz RT, Knopp A, Ogermann D, Hofmann CA, Lankl B. Optimum-capacity MIMO satellite link for fixed and mobile services. Proceedings of the International ITG Workshop on Smart Antennas; 2008:209-216; Vienna (Austria).
23. Zorba N, Realp M, Lagunas MA, Pérez-Neira AI. Dual polarization for MIMO processing in multibeam satellite systems. Proceedings of the 10th International Workshop on Signal Processing: Image Communication; 2008:1-7; Rhodes Island (Greece).
24. Arapoglou P-D, Burzigotti P, Bolea Alamanac A, De Gaudenzi R. Capacity potential of mobile satellite broadcasting systems employing dual polarization per beam. Proceedings of the Advanced Satellite Multimedia Systems Conference and the 11th Signal Processing for Space Communications Workshop (ASMS/SPSC); 2010:213-220; Cagliari (Italy).
25. Hofmann C, Storek K-U, Schwartz RT, Knopp A. Spatial MIMO over satellite: a proof of concept. Proceedings of the IEEE International Conference on Communications Kuala Lumpur (Malaysia); 2016:1-6.
26. Byman A, Hulkkonen A, Arapoglou P-D, Bertinelli M, De Gaudenzi R. MIMO for mobile satellite digital broadcasting: from theory to practice. *IEEE Trans Veh Tech*. 2016;65(7):4839-4853.
27. Alamouti SM. A simple transmit diversity technique for wireless communications. *IEEE J Sel Areas in Commun*. 1998;16(8):1451-1458.
28. Arti MK, Jindal SK. OSTBC transmission in shadowed-Rician land mobile satellite links. *IEEE Trans Veh Tech*. 2016;65(7):5771-5777.
29. Wysocki BJ, Wysocki TA. On an orthogonal space-time-polarization block code. *J Commun*. 2009;4(1):20-25.
30. Vineetha PV, Kirthiga S. Analysis of polarization diversity for land mobile satellite system. Proceedings of the International Conference Wireless Communication, Signal Processing and Networking (WiSPNET); 2017:1268-1271; Chennai (India).
31. Aparna M, Vineetha PV, Kirthiga S. Channel modeling and estimation of polarized MIMO for land mobile satellite systems. Proceedings of the International Conference on Advances in Computing, Communications and Informatics Udupi (India); 2017:299-304.
32. Xu H, Govindasamy K, Pillay N. Uncoded space-time labeling diversity. *IEEE Commun Lett*. 2016;20(8):1511-1514.
33. Quazi T, Patel SS. USTLD mapper design for APSK constellations over satellite channels. *Trans Emerging Telecomm Tech*. 2019;30(2):e3586. doi:10.1002/ett.3586
34. Patel SS, Quazi T, Xu H. A genetic algorithm for uncoded space-time labelling diversity mapper design. Proceedings of the IEEE Workshop on Signal Processing Systems; 2018:77-82; Cape Town (South Africa). doi:10.1109/sips.2018.8598435
35. Huang Y, Ritcey JA. Improved 16-QAM constellation labeling for BI-STCM-ID with the Alamouti scheme. *IEEE Commun Lett*. 2005;9(2):157-159.
36. Huang Y, Ritcey JA. Optimal constellation labeling for iteratively decoded bit-interleaved space-time coded modulation. *IEEE Trans Inf Theory*. 2005;51(5):1865-1871.
37. Patel SS, Quazi T, Xu H. High-rate uncoded space-time labeling diversity with low-complexity detection. *Int J Commun Syst*. 2020;33(8):e4520. doi:10.1002/dac.4520
38. Patel SS, Quazi T, Xu H. Error performance of uncoded space time labelling diversity in spatially correlated Nakagami-q channels. *Int J Commun Syst*. 2018;31(12):e3720. doi:10.1002/dac.3720

39. Khalid A, Quazi T, Xu H, Patel SS. Performance analysis of M-APSK generalised spatial modulation with constellation reassignment. *Int J Commun Syst*. 2020;33(14):e4497. doi:10.1002/dac.4497
40. Patel SS, Quazi T, Xu H. Performance of uncoded space-time labelling diversity in dual-correlated Rayleigh-fading channels. Proceedings of the Southern Africa Telecommunication Networks and Applications Conference (SATNAC); 2017; Barcelona (Spain).
41. Baldi M, Chiaraluce F, de Angelis A, Marchesani R, Schillaci S. A comparion between APSK and QAM in wireless tactical scenarios for land mobile systems. *EURASIP J Wirel Commun Netw*. 2012;317. doi:10.1186/1687-1499-2012-317
42. Digital Video Broadcasting. Second generation framing structure, channel coding and modulation systems for broadcasting, interactive services, news gathering and other broadband satellite applications; Part 2: DVB-S2 extensions (DVB-S2X). *Eur Telecomm Standards Inst*. 2020;26-43.
43. Quazi T, Xu H. BER performance of a hierarchical APSK UEP system over Nakagami-m fading channels. *SAIEE Africa Res J*. 2016;107(4):230-236.
44. Park B, Jin S, Jeong D, et al. Highly linear mm-wave CMOS power amplifier. *IEEE Trans Microw Theory Techn*. 2016;64(12):4535-4544.
45. Romero-Jerez JM, Lopez-Martinez FJ. A new framework for the performance analysis of wireless communications under Hoyt (Nakagami-q) fading. *IEEE Trans Inf Theory*. 2017;63(3):1693-1702.
46. Cormen TH, Leiserson CE, Rivest RL, Stein C. *Introduction to Algorithms*. Cambridge: The MIT Press; 2009.
47. Kermoal JP, Schumacher L, Pedersen KI, Mogensen PE, Frederiksen F. A stochastic MIMO radio channel model with experimental validation. *IEEE J Sel Areas Commun*. 2002;20(6):1211-1226.
48. Reşat MA, Özyurt S. Performance of zero-forcing MIMO systems with signal space diversity under transmit antenna correlation. Proceedings of the International Conference on Electrical and Electronics Engineering (ELECO); 2017:700-704; Bursa (Turkey).
49. Aalo VA. Performance of maximal-ratio diversity systems in a correlated Nakagami-fading environment. *IEEE Trans Commun*. 1995;43(8):2360-2369.
50. Albdran S, Alshammari A, Matin MA. Spectral and energy efficiency for massive MIMO systems using exponential correlation model. Proceedings of the IEEE 7th Annual Computing and Communication Workshop and Conference (CCWC); 2017; Las Vegas, NV.
51. Loyka SL. Channel capacity of MIMO architecture using the exponential correlation matrix. *IEEE Commun Lett*. 2001;5(9):369-371.
52. Patel SS, Quazi T, Xu H. Optimal antenna spacings for uncoded space-time labelling diversity systems with linear and non-linear antenna configurations. Proceedings of the Southern Africa Telecommunication Networks and Applications Conference (SATNAC); 2018:86-91; Arabella, Hermanus (South Africa).
53. Akoun PO, Xu H. Optimal error analysis of receive diversity schemes on arbitrarily correlated Rayleigh fading channels. *IET Commun*. 2016;10(7):854-861.
54. Meyer CD. *Matrix Analysis and Applied Linear Algebra*. Philadelphia: Society for Industrial and Applied Mathematics; 2000.
55. Craig JW. A new, simple, and exact result for calculating the probability of error for two-dimensional signal constellations. Proceedings of the IEEE Military Communications Conference (MILCOM); 1991:571-575; McLean, VA.
56. Hedayet A, Shah H, Nosratinia A. Analysis of space-time coding in correlated fading channels. *IEEE Trans Wirel Commun*. 2005;4(6):2882-2891.
57. Samra H, Ding Z, Hahn P. Symbol mapping diversity design for multiple packet transmissions. *IEEE Trans Commun*. 2005;53(5):810-817.
58. Seddik KG, Ibrahim AS, Liu KJR. Trans-modulation in wireless relay networks. *IEEE Commun Lett*. 2008;12(3):170-172.
59. Krasicki M. Essence of 16-QAM labelling diversity. *IET Electron Lett*. 2013;49(8):567-569.
60. Hahn PM, Grant TL. Lower bounds for the quadratic assignment problem based upon a dual formulation. *Oper Res*. 1998;46(6):912-922.
61. Hazra S, Mitra A. A new land mobile satellite channel model with Nakagami-q distribution. Proceedings of the 2012 National Conference on Communications (NCC); 2012; Kharagpur (India). doi: 10.1109/NCC.2012.6176857

How to cite this article: Patel SS, Quazi T. A multiple-input, multiple-output broadcasting system with space, time, polarization, and labeling diversity. *Trans Emerging Tel Tech*. 2022;e4663. doi: 10.1002/ett.4663